SPECIAL
Spontaneous Imbalance
COLLECTION

The Spontaneous Imbalance of an Atmospheric Vortex at High Rossby Number

DAVID A. SCHECTER

NorthWest Research Associates, Redmond, Washington

(Manuscript received 2 April 2007, in final form 12 October 2007)

ABSTRACT

This paper discusses recent progress toward understanding the instability of a monotonic vortex at high Rossby number, due to the radiation of spiral inertia–gravity (IG) waves. The outward-propagating IG waves are excited by inner undulations of potential vorticity that consist of one or more vortex Rossby waves. An individual vortex Rossby wave and its IG wave emission have angular pseudomomenta of opposite sign, positive and negative, respectively. The Rossby wave therefore grows in response to producing radiation. Such growth is potentially suppressed by the resonant absorption of angular pseudomomentum in a critical layer, where the angular phase velocity of the Rossby wave matches the angular velocity of the mean flow. Suppression requires a sufficiently steep radial gradient of potential vorticity in the critical layer. Both linear and nonlinear steepness requirements are reviewed.

The formal theory of radiation-driven instability, or "spontaneous imbalance," is generalized in isentropic coordinates to baroclinic vortices that possess active critical layers. Furthermore, the rate of angular momentum loss by IG wave radiation is reexamined in the hurricane parameter regime. Numerical results suggest that the negative radiation torque on a hurricane has a smaller impact than surface drag, despite recent estimates of its large magnitude.

1. Introduction

a. Vortex instability driven by inertia–gravity wave emission

Mesoscale vortices are among the most intriguing coherent structures in the troposphere. Figure 1 illustrates their many forms, which range from hurricanes to rotational thunderstorms. The angular velocity Ω of a mesoscale vortex typically satisfies the condition

$$f < \Omega < N, \tag{1}$$

in which f is the Coriolis parameter and N is the ambient Brunt–Väisälä frequency. This condition allows vortex-scale disturbances to resonate with ambient inertia–gravity (IG) waves, and thereby efficiently produce IG wave radiation. Recent studies have examined the magnitude of such radiation and its consequences on the vortex. This paper will review and generalize some notable results.[1]

The pertinent studies concern IG wave radiation from a monotonic cyclone (MC), whose potential vorticity (PV) consistently decays with distance from the central axis of rotation. The radial PV gradient allows Rossby-like waves to exist in the core region of the vortex (Kelvin 1880; McDonald 1968; Montgomery and Kallenbach 1997). The spectrum of vortex Rossby waves includes continuum and discrete modes. A continuum disturbance typically suffers spiral windup due to differential rotation of the mean flow. Here, we will focus on discrete vortex Rossby waves (DVRWs), which resist spiral windup and remain coherent over time. DVRWs often account for rotating tilts and elliptical (triangular, square, etc.) deformations of the vortex core. The angular phase velocity of a DVRW is of

[1] It is well known that the problems of IG wave radiation and acoustic radiation from a solitary vortex are analogous. Readers interested in the acoustic analog may consult Broadbent and Moore (1979), Kop'ev and Leont'ev (1983, 1985, 1988), Zeitlin (1991), Chan et al. (1993), and Howe (2003).

Corresponding author address: David A. Schecter, NorthWest Research Associates, 4118 148th Ave. NE, Redmond, WA 98052.
E-mail: schecter@nwra.com

DOI: 10.1175/2007JAS2490.1

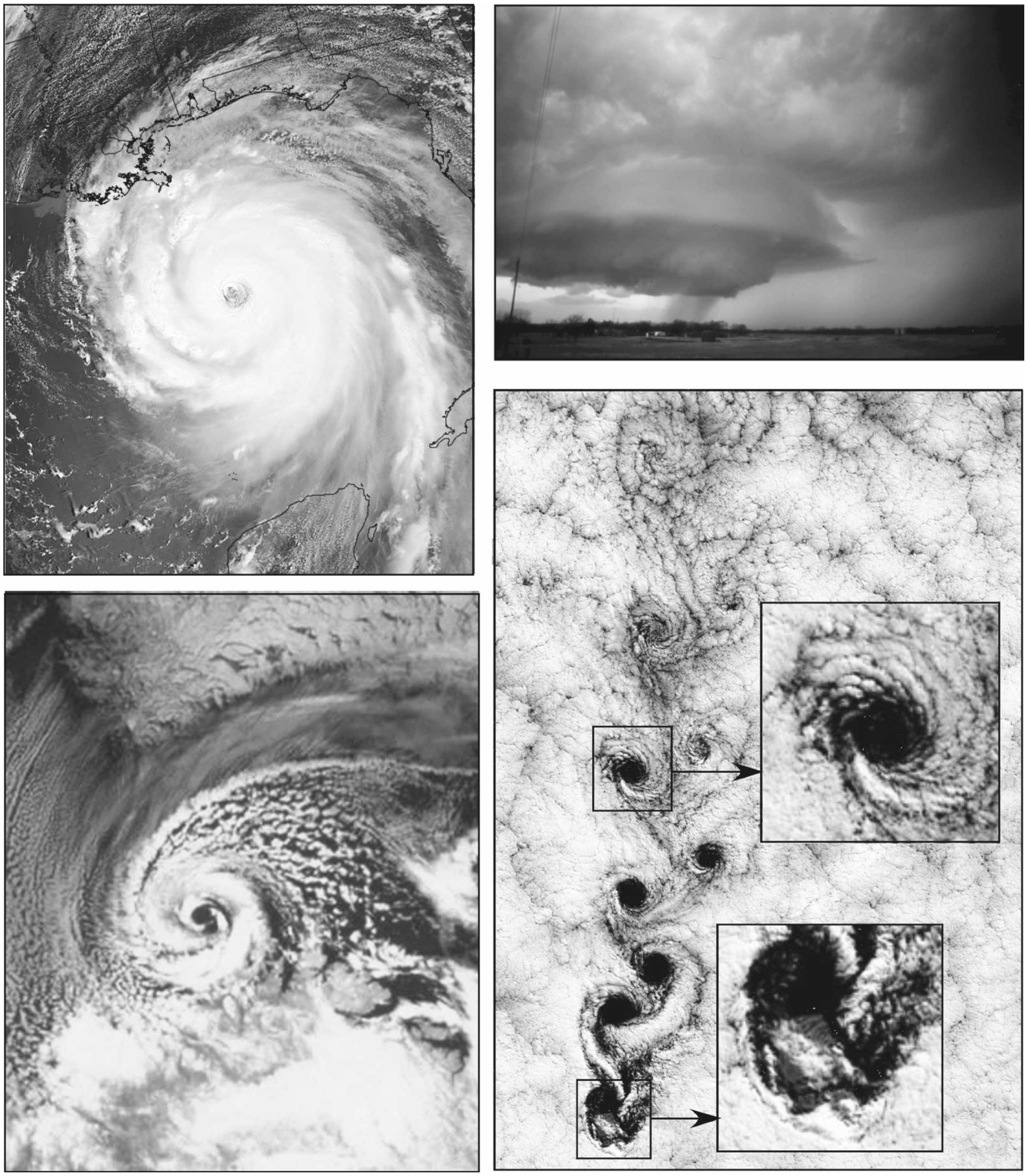

FIG. 1. It has been speculated that Rossby-like waves in vortices like these (at high Rossby and moderate-to-high Froude numbers) might produce relatively strong levels of spiral IG wave radiation. (top left) Hurricane Katrina at 0820 EDT 29 Aug 2005 (National Aeronautics and Space Administration). (top right) A mesocyclone in Duncan, OK, on 17 Mar 2003 (courtesy of Dr. Robert J. Conzemius). (bottom left) A polar low over the Barents Sea on 27 Feb 1987 (*NOAA-9*). (bottom right) Wake vortices behind Selkirk Island on 15 Sep 1999 (United States Geological Survey, Earth Resources Observation and Science; NASA).

order Ω, but is less than the angular velocity of the core circulation.

Under condition (1), a DVRW will typically excite an outward propagating spiral IG wave in the peripheral region of the vortex. Basic perturbation theory establishes that the creation of any wave by another disturbance in a circular flow must occur in such a way that conserves net angular pseudomomentum (cf. McIntyre 1981; Haynes 1988; Guinn and Schubert 1993; Shepherd 2003). It has been shown for MCs that a DVRW and its IG wave emission have angular pseudomomenta of opposite sign, positive and negative, respectively (Schecter and Montgomery 2004, hereafter SM04; Schecter and Montgomery 2006, hereafter SM06). Consequently, a DVRW must grow in response to producing radiation. By this mechanism, the core of an MC will gradually deform.

Although an atmospheric vortex is in a continuously stratified fluid, the shallow-water model suffices to explain the essential physics of the radiation-driven instability. In the context of shallow-water theory, Ford (1994a,b) verified that IG wave emissions compel cyclone-scale DVRWs in MCs to grow exponentially with time, provided that the Rossby number Ro $= \Omega/f$ exceeds unity. Ford also showed that the growth rate vanishes algebraically as the Froude number, Fr $= V/c_g$, tends to zero; here V is the azimuthal velocity of the vortex and c_g is the ambient gravity wave speed. Specifically, the maximum growth rate of a DVRW is proportional to $\mathrm{Fr}^4\Omega$ in the regime where Fr $\ll 1$. This result was later generalized by Plougonven and Zeitlin (2002) to "pancake" vortices in a continuously stratified fluid. It stands to reason that an atmospheric vortex at small Froude number would hardly feel the effects of radiation.

Nevertheless, mesoscale cyclones such as hurricanes and rotational thunderstorms (Fig. 1) can penetrate the "superspin" parameter regime, where both the Rossby and Froude numbers exceed unity. Recent numerical studies of a stratified MC indicate that superspin can shorten the *e*-folding time of a radiation-driven instability to less than four rotation periods (SM04). Chow and Chan (2003) further speculated that the spontaneous emission of spiral IG waves can remove up to one-tenth of the angular momentum of an intense hurricane in a single rotation period. A similar estimate was published earlier by Chimonas and Hauser (1997) for the negative radiation torque on a supercell mesocyclone under ideal conditions. In section 5, we will reconsider these estimates.

Of course, superspin does not guarantee that IG waves will greatly influence the evolution of a cyclone. An important mechanism for quenching the radiation-driven instability of an MC involves the resonant interaction between a DVRW and its critical layer. The critical layer of a DVRW is located beyond the core of an MC, precisely where the angular phase velocity of the wave equals the angular velocity of the mean flow. While creating radiation, a DVRW simultaneously stirs PV in its critical layer. Such stirring efficiently transfers angular pseudomomentum from the DVRW into the critical layer, and thereby acts to damp the wave. Damping will prevail over radiative pumping if the radial gradient of PV in the critical layer is sufficiently large (SM04; SM06). Figure 2 illustrates the two potential fates of a DVRW in an MC. Section 4 will demonstrate that a precise growth rate formula for the DVRW is readily extracted from an equation that expresses angular pseudomomentum conservation. For the first time, this formula will be derived for baroclinic MCs that possess active critical layers.[2]

b. *Connection to the broader problem of spontaneous imbalance*

Following the theme of the special issue for which this paper was prepared, let us now turn our attention to the general problem of spontaneous imbalance. In practical terms, balanced motions are theoretical approximations of synoptic or mesoscale flows that filter out IG waves. Quasigeostrophic (QG) flow, which applies only at small Rossby numbers, is the most familiar kind (Charney 1948; Hoskins et al. 1985; cf. Muraki et al. 1999). More general forms of balanced flow are contained in the semigeostrophic model (Hoskins 1975; Hoskins et al. 1985), the standard balance model (McWilliams 1985), and the asymmetric balance model (Shapiro and Montgomery 1993). Spontaneous imbalance (SI) is the divergence of an actual flow from the predictions of a balance model, which usually involves the production of IG waves. SI is evident in numerical simulations of baroclinic instability and frontogenesis (Snyder et al. 1993; O'Sullivan and Dunkerton 1995; Griffiths and Reeder 1996; Reeder and Griffiths 1996; Zhang 2004; Plougonven and Snyder 2005). At Ro $\ll 1$, theoretical arguments suggest that balanced motions will produce exponentially weak IG wave emissions (Saujani and Shepherd 2002; Vanneste and Yavneh 2004). At high Rossby numbers, compact regions of unsteady balanced motions can resonate more directly with environmental IG waves and thereby exhibit stronger SI (Ford et al. 2000, 2002).

Typically, the intrinsic frequency of a DVRW will not exceed the characteristic inertial frequency of the vortex in which it resides, regardless of the Rossby number (cf. Montgomery and Lu 1997). From this local perspective, it is sensible to approximate DVRWs with a model that filters out IG waves. Section 2 will review the interaction of a DVRW with its critical layer in the context of the asymmetric balance (AB) model, which ostensibly applies to hurricanes as well as quasigeostrophic cyclones. However, at high Rossby number the

[2] It is notable that the theory of modal growth in astrophysical disks must likewise treat the net influence of critical layer stirring and spiral density wave radiation. See, for example, Papaloizou and Pringle (1987) and Shukhman (1991).

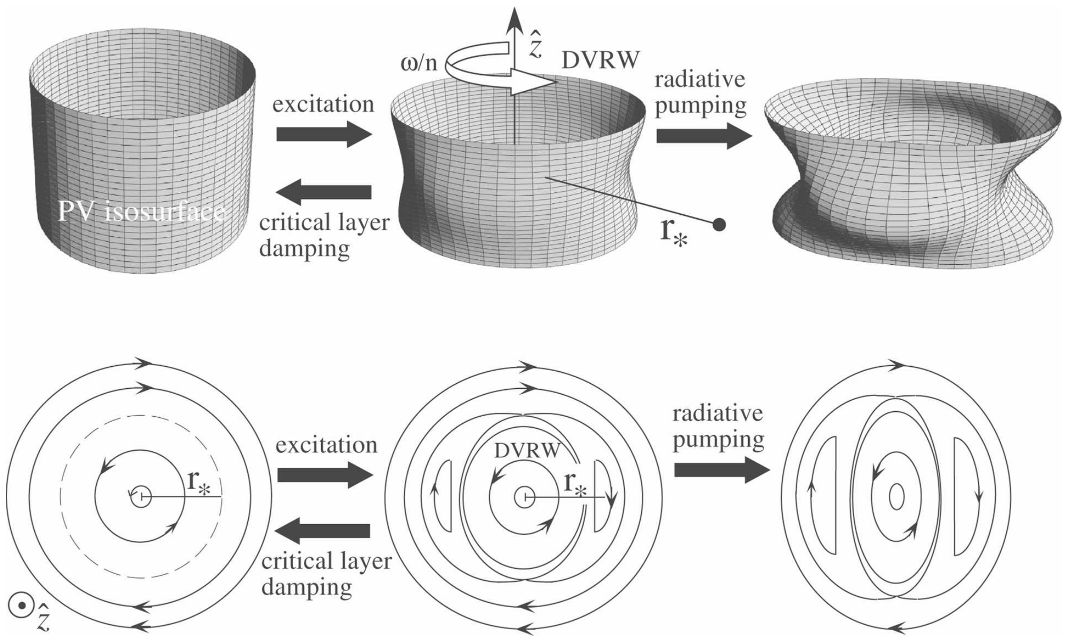

FIG. 2. The two potential fates of a DVRW in the core of a stratified MC, bounded above and below by rigid surfaces (cf. Schecter and Montgomery 2003; SM04). Evolution (top) of a PV isosurface deformed by the DVRW and (bottom) of the horizontal flow at fixed height z in a reference frame that corotates with the DVRW. An initial perturbation of the balanced cyclone (middle) excites a baroclinic DVRW with azimuthal wavenumber $n = 2$ and angular phase velocity ω/n. The DVRW excites an outward propagating spiral IG wave in the environment, and stirs PV in its critical layer at $r = r_*$. If the positive feedback of IG wave radiation prevails, the DVRW will grow (left to right). If the negative feedback of PV stirring prevails, the DVRW will decay (right to left).

balance approximation is unjustifiable in the far field where the inertial frequency reduces to f. As explained previously, this allows a DVRW to match onto an outward propagating spiral IG wave. The balance approximation will qualitatively fail for the DVRWs of MCs if critical layer damping is unable to restrain the positive feedback of IG wave radiation (see section 3). In this sense, the radiation-driven instability of an MC is a prime example of SI.

c. Outline

The remainder of this paper is organized as follows. Section 2 qualitatively reviews the balanced interaction of a DVRW and its critical layer in a shallow-water MC. Section 3 examines both linear and nonlinear conditions for the SI of a shallow-water MC. Section 4 derives a formula for the growth rate of a DVRW near marginal stability in a baroclinic MC. This formula accounts for the positive feedback of IG wave emission and the negative feedback of PV stirring in a 3D critical layer. Section 5 reexamines the torque that is applied by spontaneous radiation on a barotropic cyclone with parameters similar to those of a category 5 hurricane. Section 6 summarizes the main text and suggests future lines of investigation. For convenient reference, the appendices review the standard primitive equations that form the theoretical foundation of this paper.

2. The balanced evolution of a discrete vortex Rossby wave

This section qualitatively reviews the balanced interaction of a DVRW with its critical layer. For simplicity, we will limit our discussion to linear shallow-water theory on the f plane. Throughout, we will refer to a polar coordinate system whose origin is at the center of the vortex. As usual, the symbols r, φ, and t will denote radius, azimuth, and time. A generic flow field $h(r, \varphi, t)$ will be separated into a basic state $\overline{h}(r)$ and a perturbation $h'(r, \varphi, t)$.

a. The unperturbed cyclone

By definition, the basic state of the vortex satisfies gradient balance; that is,

$$\overline{u} = 0 \quad \text{and} \quad \frac{d\overline{\phi}}{dr} = \frac{\overline{\upsilon}^2}{r} + f\overline{\upsilon}, \tag{2}$$

in which $\overline{u}$ is the radial velocity, $\overline{\upsilon}$ is the azimuthal velocity, $\overline{\phi}$ is the geopotential, and f is the constant Coriolis parameter. For notational convenience, we introduce the following auxiliary variables:

$$\overline{\Omega} \equiv \overline{\upsilon}/r, \quad \overline{\zeta} \equiv r^{-1} d(r\overline{\upsilon})/dr,$$
$$\overline{\eta} \equiv \overline{\zeta} + f, \quad \overline{\xi} \equiv 2\overline{\Omega} + f, \tag{3}$$

in which $\overline{\Omega}$ is the angular rotation frequency, $\overline{\zeta}$ is the relative vertical vorticity, $\overline{\eta}$ is the absolute vertical vorticity, and $\overline{\xi}$ is the modified Coriolis parameter. The basic-state potential vorticity is defined by

$$\overline{q} \equiv \overline{\eta}/\overline{\phi}. \tag{4}$$

As mentioned earlier, the radial gradient of $\overline{q}$ supports the existence of vortex Rossby waves. Unless stated otherwise, we will assume that the basic state has the following properties:

(i) $\overline{q}$ is uniformly positive,
(ii) $d\overline{q}/dr$ is uniformly negative, and
(iii) $d\overline{\Omega}/dr$ is uniformly negative.

Conditions (i)–(iii) define a monotonic cyclone (MC).

b. *The asymmetric balance model for weak perturbations*

Disturbances to the basic state are exactly governed by the primitive equations (appendix A). Standard balance approximations of the primitive equations rely upon the smallness of the Rossby number, the Froude number, or both (cf. McWilliams 1985; Polvani et al. 1994). Here, we consider an alternative that has become somewhat popular in hurricane meteorology. To begin with, let us classify perturbations according to the magnitude of

$$\mathcal{D}^2 \equiv \left(\frac{\partial}{\partial t} + \overline{\Omega}\frac{\partial}{\partial \varphi}\right)^2 \bigg/ \overline{\eta}\,\overline{\xi}. \tag{5}$$

The value of $\mathcal{D}^2$ is the squared rate of change of the disturbance in a reference frame that follows the basic flow, divided by the regional inertial stability. Loosely speaking, vortex Rossby waves satisfy $\mathcal{D}^2 < 1$, whereas IG waves satisfy $\mathcal{D}^2 > 1$ (cf. Montgomery and Lu 1997). In other words, vortex Rossby waves are intrinsically slow, whereas IG waves are intrinsically fast. For low azimuthal wavenumbers, and Rossby numbers of order unity or less, the vortex Rossby waves of a cyclone typically satisfy the more restrictive condition that

$$\mathcal{D}^2 \ll 1. \tag{6}$$

Condition (6) is the cornerstone of the AB model, which filters out IG waves and provides a reduced set of equations for vortex Rossby wave dynamics in ageostrophic vortices (Shapiro and Montgomery 1993; Montgomery and Franklin 1998; Ren 1999; Möller and Shapiro 2002; McWilliams et al. 2003).

It is straightforward to derive the lowest-order AB model from the linearized primitive equations. To simplify notation, let

$$\frac{D_V}{Dt} \equiv \frac{\partial}{\partial t} + \overline{\Omega}\frac{\partial}{\partial \varphi}. \tag{7}$$

Operating on both sides of the linearized momentum equations with D_V/Dt yields

$$u' = -\frac{1}{\overline{\eta}}\left(\frac{1}{r}\frac{\partial \phi'}{\partial \varphi} + \frac{1}{\overline{\xi}}\frac{D_V}{Dt}\frac{\partial \phi'}{\partial r}\right) - \mathcal{D}^2 u',$$
$$\upsilon' = \frac{1}{\overline{\xi}}\left(\frac{\partial \phi'}{\partial r} - \frac{1}{r\overline{\eta}}\frac{D_V}{Dt}\frac{\partial \phi'}{\partial \varphi}\right) - \mathcal{D}^2 \upsilon' \tag{8}$$

in which u' is the radial velocity perturbation, υ' is the azimuthal velocity perturbation, and ϕ' is the geopotential perturbation. Substituting the right-hand sides of Eqs. (8) into the linearized potential vorticity equation (McWilliams et al. 2003), and neglecting terms of order $\mathcal{D}^2$ and higher yields

$$\frac{D_V \hat{q}'}{Dt} = \frac{1}{r}\frac{d\overline{q}}{dr}\frac{1}{\overline{q}^2}\frac{\partial \phi'}{\partial \varphi}. \tag{9}$$

Here we have introduced the quasi–potential vorticity perturbation,

$$\hat{q}' \equiv \frac{1}{r}\frac{\partial}{\partial r}\left(r l_D^2 \frac{\partial \phi'}{\partial r}\right) + \frac{l_D^2 \overline{\nu}}{r^2}\frac{\partial^2 \phi'}{\partial \varphi^2} - \phi', \tag{10}$$

in which

$$l_D(r) \equiv \sqrt{\frac{\overline{\phi}}{\overline{\eta}\,\overline{\xi}}} \tag{11}$$

is a local deformation radius, and $\overline{\nu}(r) = (2\overline{\xi} - \overline{\eta})/\overline{\eta}$.[3] Equation (9) is the only prognostic equation in the AB model. By Eq. (10), it is essentially an equation for the temporal evolution of ϕ'. Equations (8) reduce to diagnostic formulas for u' and υ' by neglecting the far right terms that are proportional to $\mathcal{D}^2$.

[3] The original derivation of the AB model (Shapiro and Montgomery 1993) followed a different path, which resulted in $\overline{\nu} = 1$. This discrepancy has no bearing on the present discussion, and becomes negligible for small but finite Rossby numbers. Different AB models are possible because their derivation paths tacitly require different secondary conditions of validity.

Note that the AB model [Eqs. (9)–(10)] conveniently retains QG structure at high Rossby number. Furthermore, if the Rossby and Froude numbers satisfy the relation $\mathrm{Fr}^2 \ll \mathrm{Ro} \ll 1$, the AB model properly reduces to the QG model. That is, (u', v') becomes the geostrophic velocity perturbation, l_D becomes the constant Rossby deformation radius l_R, and $\hat{q}'$ becomes l_R^2 times the quasigeostrophic PV perturbation.

c. Basic kinematics of the DVRW–critical layer interaction

A DVRW has a quasi-PV distribution of the form

$$\hat{q}'_d = a(t)\hat{Q}(r)e^{i(n\varphi - \omega t)} + \text{c.c.}, \tag{12}$$

in which a is the complex wave amplitude, n is the azimuthal wavenumber, and c.c. denotes the complex conjugate of the preceding term. We will assume that the complex radial wavefunction $\hat{Q}$ vanishes beyond some core radius. We will further assume that the phase of a varies at a much slower rate than the real wave frequency ω. Note that a DVRW has fixed radial structure and therefore differs from a generic continuum disturbance that is sheared by the differential rotation of the mean flow (e.g., Montgomery and Kallenbach 1997; Bassom and Gilbert 1998; Brunet and Montgomery 2002; McWilliams et al. 2003).

In the outer region of the vortex, there is a critical layer where the phase velocity of the DVRW equals the angular rotation frequency of the mean flow. The central radius r_* of the critical layer is precisely defined by the resonance condition

$$\overline{\Omega}(r_*) \equiv \omega/n. \tag{13}$$

Figure 3a illustrates a typical set of critical layers for the DVRWs of a shallow-water MC.

Through the extension of its velocity field, the DVRW can stir fluid everywhere beyond the core. Outside of the critical layer, fluid parcels moving with the mean flow experience rapid oscillations of positive and negative wave forcing, which will have little cumulative effect on the amplitude of $\hat{q}'$. Within the critical layer, fluid parcels are essentially phase locked with the wave. It is therefore reasonable to assert that a DVRW will most profoundly disturb $\hat{q}'$ in the neighborhood of r_* and that we need only consider the interaction between a DVRW and its critical layer (cf. Lansky et al. 1997).

Any interaction between different components of the perturbation must conserve total angular pseudomomentum. In AB theory, the angular pseudomomentum is given by

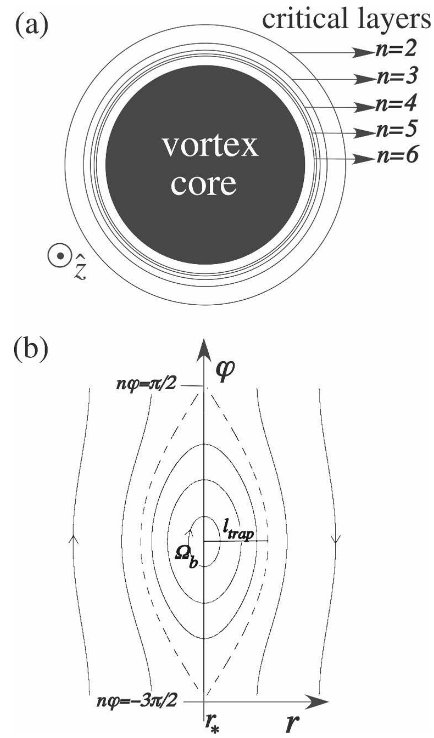

FIG. 3. (a) Typical arrangement of the critical layers of the DVRWs of a shallow-water MC. The central radius r_* of the critical layer decreases as the azimuthal wavenumber n increases. (b) Instantaneous streamlines in the critical layer of a DVRW, viewed in a reference frame that corotates with the wave. The symbol Ω_b denotes the orbital angular frequency of fluid parcels near the center of the cat's eye, and l_{trap} denotes the half-width of the trapping region that is enclosed by the separatrix. Both Ω_b and l_{trap} are proportional to the square root of the wave amplitude, which can vary with time.

$$L^{(\mathrm{AB})} \equiv \int d\mathbf{x}^2 \frac{r(\overline{q}\hat{q}')^2}{-2d\overline{q}/dr}, \tag{14}$$

in which the integral is over all space (Ren 1999). Note that $L^{(\mathrm{AB})}$ is positive definite because we have assumed that $d\overline{q}/dr$ is uniformly negative. If only the DVRW and critical layer contribute significantly to $L^{(\mathrm{AB})}$, its conservation law reduces to

$$\frac{d}{dt}\int_{\text{core}} d\mathbf{x}^2 \frac{r(\overline{q}\hat{q}'_d)^2}{-2d\overline{q}/dr} = -\frac{d}{dt}\int_{\text{cl}} d\mathbf{x}^2 \frac{r(\overline{q}\hat{q}'_{\text{cl}})^2}{-2d\overline{q}/dr}, \tag{15}$$

in which the left integral is over the area of the vortex core and the right integral is over the area of the critical layer. For convenience, we have introduced the notation $\hat{q}'_{\text{cl}}$ to represent $\hat{q}'$ in the critical layer. Suppose that $\hat{q}'_{\text{cl}}$ is initially zero and then grows under the influence of the DVRW. According to Eq. (15), the DVRW must

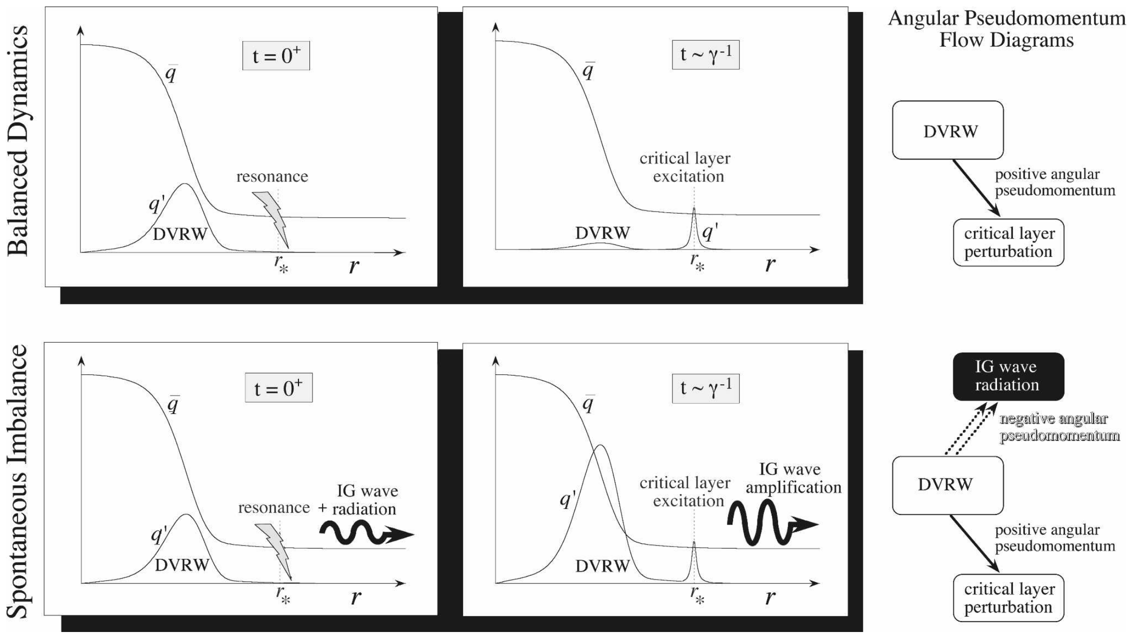

FIG. 4. (top) Balanced dynamics of a DVRW. In a balance model, the core DVRW resonantly excites a PV perturbation at the critical radius r_*. To conserve total angular pseudomomentum, the DVRW must decay. (bottom) Spontaneous imbalance. If the Rossby number exceeds unity, the DVRW will also emit a frequency-matched spiral IG wave into the environment. Since the IG wave has negative angular pseudomomentum, its creation compels the DVRW to grow. In this cartoon, radiative pumping dominates critical layer damping of the DVRW and causes an instability that is a form of spontaneous imbalance. In both panels, the symbol γ represents the characteristic growth/decay rate of the DVRW. Note also that $\overline{q}$ is sketched for spatial reference only, and is not drawn to scale relative to q' in the vertical.

decay in response. Figure 4 (top) illustrates the kinematics.[4]

The reader may have noticed that a damped DVRW cannot possibly be an eigenmode of an MC. An eigenmode consists of a $\hat{q}'$ distribution that decays exponentially with time everywhere in space. In contrast, a DVRW decays because of growing $\hat{q}'_{\text{cl}}$. For this reason, and others that are more technical, the DVRWs of MCs are more properly classified as "quasi-modes" (Briggs et al. 1970; Corngold 1995; Spencer and Rasband 1997). If the vortex were nonmonotonic, then $d\overline{q}/dr$ could have opposite signs in the core and at r_*. According to Eq. (15), the DVRW would then grow in response to its action on the critical layer (Briggs et al. 1970; Schecter et al. 2000, 2002; Benilov 2005; Mallen et al. 2005). Simultaneous growth of a DVRW and $\hat{q}'_{\text{cl}}$ is consistent with the behavior of a genuine eigenmode.

[4] The resonant damping of a DVRW is analogous to the "Landau damping" of a discrete plasma wave (Landau 1946; O'Neil 1965). Moreover, in nonneutral plasma physics the resonant damping of a DVRW is known as the Landau damping of a diocotron (slipping stream) mode (Briggs et al. 1970; cf. Davidson 1990, chapter 6).

3. The spontaneous imbalance of a shallow-water cyclone

a. *The positive feedback of spiral radiation*

At Rossby numbers greater than unity, any DVRW of a shallow-water MC can excite a frequency-matched outward propagating spiral IG wave in the environment. In other words, the geopotential (and velocity components) of the balanced DVRW can match onto a spiral IG wave at the periphery of the circular flow. As mentioned earlier, the spiral radiation has positive feedback on the DVRW.

We may understand the positive feedback by reconsidering conservation of angular pseudomomentum. To lowest order in the perturbation fields, the angular pseudomomentum of an unfiltered perturbation in a shallow-water cyclone is given by (cf. Guinn and Schubert 1993)

$$L^{(\text{SW})} \equiv \int d\mathbf{x}^2 \jmath^{(\text{SW})}, \tag{16}$$

in which the area integral is over all space, and

$$\jmath^{(\text{SW})} \equiv \frac{r\overline{\phi}^2(q')^2}{-2d\overline{q}/dr} - rv'\phi'. \tag{17}$$

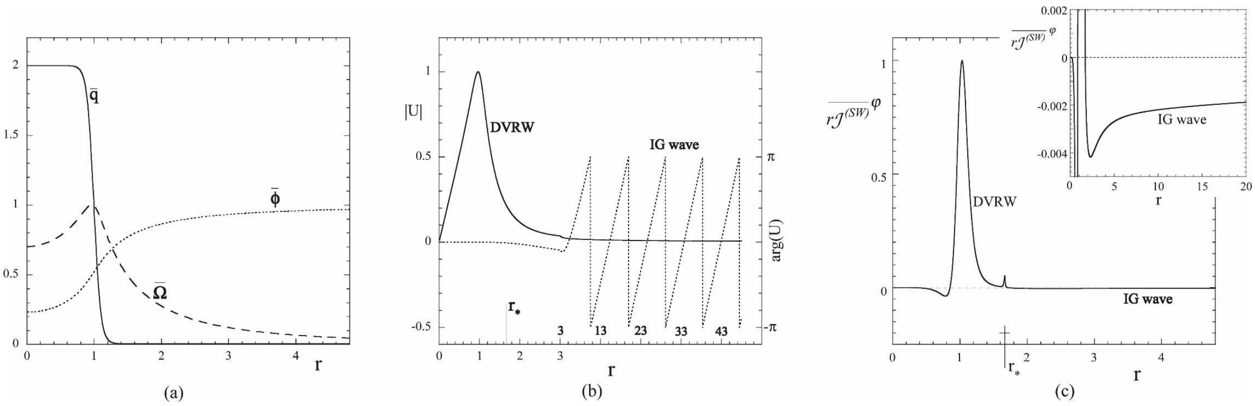

FIG. 5. The radial structure of an SI mode. (a) The basic state of the shallow-water cyclone that suffers SI. The radial coordinate r is normalized to the characteristic vortex scale r_o. The variables $\overline{\Omega}$ and $\overline{\phi}$ are in units of $\overline{\Omega}_{\max}$ and the ambient geopotential ϕ_a. The potential vorticity $\overline{q}$ is normalized to one-half of its peak value. The Rossby number of the cyclone is $\mathrm{Ro} \equiv \overline{\Omega}_{\max}/f = 53$, and the squared Froude number is $\mathrm{Fr}^2 \equiv (\overline{\Omega}_{\max} r_o)^2/\phi_a = 0.74$. (b) The magnitude (solid curve) and phase (dotted curve) of the radial velocity wavefunction U of the $n = 2$ SI mode. The magnitude is normalized to have a peak value of 1. (c) The azimuthally averaged angular pseudomomentum density $\overline{r\mathcal{J}^{(\mathrm{SW})}}^{\varphi}$ of the mode, normalized to its peak value at the instant under consideration. The DVRW and IG wave components have positive and negative angular pseudomomenta, respectively. The bump at r_* accounts for the absorption of wave activity by the critical layer. In this case, radiative pumping prevails over critical layer damping, but is fairly weak. The growth rate γ of the mode is merely $0.007\overline{\Omega}_{\max}$.

The first component of $\mathcal{J}^{(\mathrm{SW})}$ is proportional to the square of the exact PV perturbation q' and corresponds to the angular pseudomomentum density that appears in most balance models. The new term, proportional to $v'\phi'$, has emerged by the removal of balance constraints.

With the addition of radiation, conservation of angular pseudomomentum now takes the form

$$\frac{d}{dt}\int_{\mathrm{core}} d\mathbf{x}^2 \mathcal{J}_d^{(\mathrm{SW})} = -\frac{d}{dt}\int_{\mathrm{env}} d\mathbf{x}^2 \mathcal{J}_{\mathrm{rad}}^{(\mathrm{SW})} - \frac{d}{dt}\int_{\mathrm{cl}} d\mathbf{x}^2 \mathcal{J}_{\mathrm{cl}}^{(\mathrm{SW})}. \quad (18)$$

The integral on the left-hand side of Eq. (18) covers the core DVRW. The top integral on the right-hand side covers the environmental radiation field, whereas the bottom integral covers the critical layer disturbance. It has been shown that the PV component of $\mathcal{J}_d^{(\mathrm{SW})}$ dominates the angular pseudomomentum of the DVRW, and yields a *positive* integral (SM06). On the other hand, the $v'\phi'$ component of $\mathcal{J}_{\mathrm{rad}}^{(\mathrm{SW})}$ dominates the angular pseudomomentum of the spiral IG wave radiation, and yields a *negative* integral (SM06). Hence, by exciting a spiral IG wave, the DVRW creates angular pseudomomentum of opposite sign. Neglecting the critical layer, the DVRW must grow in response. In other words, the top term on the right-hand side of Eq. (18) is positive. Figure 4 (bottom) illustrates the spontaneous growth of a DVRW due to the emission of an IG wave that has negative angular pseudomomentum. Such growth is in sharp contrast to balanced dynamics, where the DVRW is either neutral or damped.

Figure 5 contains a snapshot of an exponentially growing SI mode of a shallow-water cyclone at $\mathrm{Fr}^2 = 0.74$ and $\mathrm{Ro} = 53$ (cf. SM06). For reference, Fig. 5a shows the basic state of the cyclone, which possesses a monotonic potential vorticity distribution. The angular velocity of the basic state is slightly nonmonotonic, but this feature is unimportant for our discussion. Figure 5b shows the complex radial velocity wavefunction U of the SI mode, which is defined by $u' = a(t)U(r)e^{i(n\varphi - \omega t)} +$ c.c. The inner part of U corresponds to a DVRW, and maintains an approximately constant phase far beyond the critical radius r_*. The outer part of U corresponds to a spiral IG wave and has increasing phase with radius. Figure 5c verifies that the angular pseudomomenta of the DVRW and IG wave are positive and negative, respectively. Because the Froude number of the cyclone is less than unity, the IG wave emission is fairly weak. Consequently, the e-folding time of the SI mode is many (23) vortex rotation periods.

In the parameter regime where the vortex motion is approximately governed by 2D Euler flow, say $f = 0$ and $\mathrm{Fr}^2 \ll 1$, the radiation-driven instability is readily explained in more familiar terms. In the 2D Euler model, the conserved potential vorticity reduces to $q = \zeta/\phi_a$ in which ϕ_a is the constant ambient geopotential. Furthermore, the mean torque per unit mass on the cyclone at the radius r is given to lowest order by

$$\frac{\partial}{\partial t} r\overline{v}^{\varphi} = -r\overline{\zeta u}^{\varphi} = \frac{\partial}{\partial t}\frac{r\phi_a\overline{(q')^2}^{\varphi}}{2d\overline{q}/dr}, \tag{19}$$

in which $\overline{h}^{\varphi}$ is the azimuthal average of h. Equation (19) indicates that an MC (in which $d\overline{q}/dr < 0$) will lose angular momentum as a DVRW $[(q')^2]$ grows. It is therefore sensible that the outward angular momentum flux of IG wave radiation acts to amplify the DVRW.

b. The growth rate of a DVRW and its coupled radiation field

Of course, an instability will occur only if the positive feedback of IG wave radiation prevails over the negative feedback of PV stirring in the critical layer. In section 4, we will derive a fairly general solution for the growth rate of a DVRW in a baroclinic cyclone that accounts for both feedbacks. Here we cite a closed-form result (based on linear perturbation theory) for the growth rate of a DVRW in a special shallow-water cyclone whose relative PV distribution consists of a constant core, surrounded by a low amplitude skirt. Specifically, let

$$\overline{q} = \frac{f}{\phi_a} + \frac{2\Omega_o}{\phi_a}\begin{cases} 1, & r < r_o, \\ \alpha(r), & r > r_o, \end{cases} \tag{20}$$

in which Ω_o is a positive constant, $\alpha \ll 1$, and $d\alpha/dr < 0$. For simplicity, we will again suppose that $f = 0$ and $\mathrm{Fr}^2 \ll 1$. In this case, a Rankine circulation is an excellent approximation of the basic flow out to very large distances; that is,

$$\overline{v}(r) \simeq \Omega_o r_o \frac{r_<}{r_>} \tag{21}$$

in which $r_>$ ($r_<$) is the greater (lesser) of r and r_o. Furthermore, the frequency and critical radius of the nth DVRW are given by

$$\omega = \Omega_o(n-1) \quad \text{and} \quad r_* = r_o\sqrt{\frac{n}{n-1}} \tag{22}$$

to zero order in Fr^2 and α (Kelvin 1880; Briggs et al. 1970; Ford 1994a).

After a brief transition period, the amplitude of a DVRW in the cyclone under consideration obeys an equation of the form

$$\frac{d|a|}{dt} = \gamma|a|, \tag{23}$$

in which[5]

$$\gamma = \frac{\pi n(n-1)^{2n}}{(n!)^2 2^{2n}}\mathrm{Fr}^{2n}\Omega_o + \frac{\pi}{4n}\left(\frac{n-1}{n}\right)^{n-3/2}\phi_a r_o\left(\frac{d\overline{q}}{dr}\right)_{r=r_*} \tag{24}$$

for $n \geq 2$, and $\gamma = 0$ for the $n = 1$ pseudomode that corresponds to a static displacement. As in the more general case of section 4, the first (top) term of the growth rate γ accounts for the positive feedback of IG wave radiation (cf. Ford 1994a). Its magnitude decreases algebraically with the Froude number, $\mathrm{Fr} = \Omega_o r_o/\sqrt{\phi_a}$. The second (bottom) term accounts for the negative feedback of the critical layer disturbance (cf. Briggs et al. 1970). It is directly proportional to the negative radial gradient of basic-state PV at r_*. This is because a steeper gradient at r_* permits stirring (the radial redistribution of fluid elements) to create a larger PV perturbation in the critical layer. Equivalently, a steeper gradient at r_* increases the capacity of the critical layer to absorb angular pseudomomentum.

It is important to emphasize that Eq. (23), in which γ is constant, corresponds to linearized dynamics. Henceforth, γ will refer exclusively to the growth rate of a DVRW in linear theory.

c. Nonlinear SI

Suppose that linear theory predicts the exponential decay of a DVRW, because the radial gradient of $\overline{q}$ is steep at the critical radius r_*. Nonlinear dynamics allows $\overline{q}$, interpreted as the azimuthal mean of q, to change with time (cf. Killworth and McIntyre 1985; Maslowe 1986). In nonlinear balance models, $d\overline{q}/dr$ at r_* tends to oscillate and become negligible, provided that the initial DVRW amplitude exceeds a threshold. Equation (24) suggests that leveling of $\overline{q}$ at r_* would enable radiative pumping to prevail over critical-layer damping.

The amplitude threshold that is required to "flatten" $\overline{q}$ in the critical layer has been examined theoretically (Briggs et al. 1970; Balmforth et al. 2001; cf. Le Dizes 2001), numerically (Bachman 1998; SM06; cf. Rossi et al. 1997), and experimentally (Pillai and Gould 1994; Cass 1998; Schecter et al. 2000). A good estimate for this threshold is obtained by considering basic critical layer dynamics. Figure 3b shows that the critical layer contains a region where fluid parcels (within one azi-

[5] Schecter et al. 2008 contains an explicit derivation and numerical verification of the acoustic analog of Eq. (24).

muthal wavelength) are bound to orbit a central fixed point. The region of trapped fluid is enclosed by a separatrix. The radial width of the separatrix is given by

$$l_{\text{trap}} \equiv 2\left|\frac{2aU}{nd\overline{\Omega}/dr}\right|^{1/2}_{r=r_*}, \tag{25}$$

in which $|2aU|$ is the peak radial velocity of the DVRW at a given radius (cf. section 3a). The orbital angular frequency of a trapped fluid parcel has a characteristic value of order

$$\Omega_b \equiv |2naUd\overline{\Omega}/dr|^{1/2}_{r=r_*}, \tag{26}$$

which is commonly called the "bounce frequency." In linear theory, both l_{trap} and Ω_b decrease exponentially with time, in proportion to the square root of $a = a_o e^{\gamma t}$.

Linear theory tacitly assumes that trapped fluid parcels move outside of the collapsing separatrix before making too much progress along their orbital cycles. The escape of trapped fluid prevents thorough mixing of PV. However, if the initial bounce frequency exceeds the linear decay rate of the wave; that is, if

$$\Omega_b(a_o) \gtrsim |\gamma|, \tag{27}$$

then trapped fluid parcels would complete their orbital cycles and collectively coil PV inside the separatrix. Such coiling tends to level $\overline{q}$ in the vicinity of r_* and thereby arrest critical layer damping. In other words, condition (27) is sufficient grounds for a nonlinear radiation-driven instability.

An alternative line of reasoning leads to the same conclusion. Let us first posit that a nonlinear radiation-driven instability will occur if the initial angular pseudomomentum of the DVRW exceeds the finite absorption capacity of the critical layer. Assuming that the PV component dominates the angular pseudomomentum, this condition can be written

$$\int_0^{2\pi}\int_0^{r_c} d\varphi\, dr \frac{r^2\overline{\phi}^2(q_d')^2}{-2d\overline{q}/dr}\Bigg|_{t=0} \geq \max\left(\int_0^{2\pi}\int_{r_*-\delta r_*}^{r_*+\delta r_*} d\varphi\, dr\frac{r^2\overline{\phi}^2(q_{\text{cl}}')^2}{-2d\overline{q}/dr}\right), \tag{28}$$

in which $r_c < (r_* - \delta r_*)$ is the radius of the vortex core, and δr_* is the half-width of the critical layer. As usual, the subscripts d and cl refer to the DVRW and critical-layer perturbation, respectively.

To estimate the right-hand side of the above inequality, we may first suppose that

$$\max[(q_{\text{cl}}')^2] \sim \left(\delta r_* \frac{d\overline{q}}{dr}\right)^2_{r=r_*}. \tag{29}$$

The above estimate for q_{cl}' follows from material conservation of PV. In addition, we may suppose that

$$\delta r_* \sim \max(l_{\text{trap}}, l_\gamma). \tag{30}$$

The above estimate for δr_* considers two possibilities. The first candidate l_{trap} is the initial half-width of the separatrix [Eq. (25)]. The second candidate l_γ is derived from linear theory; it is the radial length scale of the peak that develops in q_{cl}' as $t \to \infty$. Schecter et al. (2000) demonstrates that, to lowest order in γ,

$$l_\gamma = \left|\frac{\gamma}{nd\overline{\Omega}/dr}\right|_{r=r_*}. \tag{31}$$

If $\gamma \ll \omega$ and the correction to balanced dynamics is small, then we may infer from SM06 (cf. section 4) that

$$\gamma \approx \frac{\pi}{\displaystyle\int_0^{r_c} dr \frac{r^2\overline{\phi}^2|Q|^2}{-d\overline{q}/dr}}\left(\frac{r^2|U|^2\overline{\phi}^2 d\overline{q}/dr}{|nd\overline{\Omega}/dr|}\right)_{r=r_*}. \tag{32}$$

Using $q_d' = a_o Q(r)e^{in\varphi}$ + c.c. at $t = 0$, Eq. (32) for γ, and either l_{trap} or l_γ for δr_*, condition (28) amounts to (27) up to an undetermined constant of proportionality on, say, the right-hand side.

d. An illustrative numerical simulation

Figures 6–8 (adapted from SM06) illustrate the nonlinear SI of a numerically simulated shallow-water MC. The initial condition consists of a balanced elliptical deformation of the vortex core. Figure 6 shows the evolution of the potential vorticity field and the asymmetric component of the geopotential perturbation. The core perturbation consists of an $n = 2$ DVRW, which over time generates an outward propagating spiral IG wave in the far field. Early on, PV stirring in the critical layer (which appears as filamentation) tends to damp the DVRW and its radiation field. Later on, the DVRW and IG wave spontaneously amplify. The bottom panel of Fig. 6 provides a detailed picture of PV stirring in the critical layer. In time, trapped fluid parcels collectively coil the PV distribution into a pattern that is said to resemble a pair of cat's eyes.

Figure 7 (top solid curve) shows a time series of the amplitude of the DVRW. For analytical purposes, the ratio $|\Omega_b/\gamma|^2$ is substituted for a dimensional measure of the perturbation strength. Initially, the DVRW decays exponentially with time, exactly as predicted by

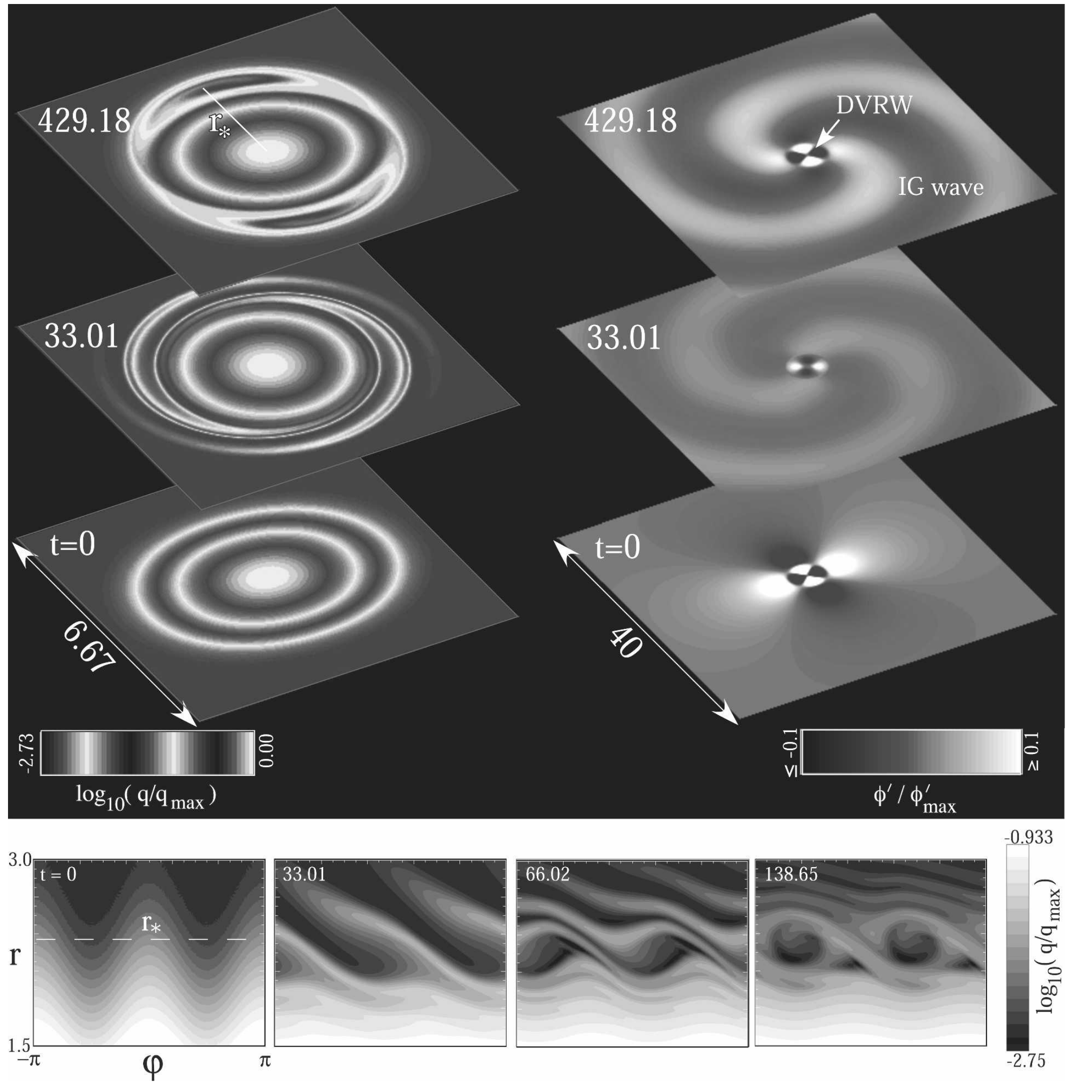

FIG. 6. Numerical simulation of the nonlinear SI of a shallow-water MC on the f plane. (top left) Evolution of the PV distribution q. Note that core ellipticity (the DVRW) decays and then grows. (top right) Evolution of the asymmetric component of the geopotential perturbation ϕ'. Note that ϕ' decays and then grows. (bottom) Detailed evolution of the PV distribution in the critical layer. For all panels, time t is measured in units of $\overline{\Omega}_{\max}^{-1}$, and lengths are normalized to a characteristic vortex-scale r_o. The Rossby number of the cyclone is $\mathrm{Ro} \equiv \overline{\Omega}_{\max}/f = 40$, and the Froude number is $\mathrm{Fr} \equiv \overline{\Omega}_{\max} r_o/\sqrt{\phi_a} = 0.7$. The data shown here correspond to simulation G1 of SM06.

linear theory (top dashed curve). Since the initial value of Ω_b exceeds the magnitude of γ, the time series eventually diverges from linear theory. Specifically, the amplitude of the DVRW bounces after a time period of order $2\pi/\Omega_b$. At this point, the critical layer starts to periodically return a fraction of the angular pseudomomentum that it absorbs. As a result, critical layer damping becomes inefficient. In the meantime, the positive feedback of IG wave radiation remains steady. Ultimately, radiative pumping prevails and SI ensues.

The bottom curves in Fig. 7 show the nonlinear (solid) and linear (dashed) evolution of the mode amplitude in a similar experiment in which the initial value of Ω_b is less than the magnitude of γ. In contrast to the previous case, cat's eyes do not fully develop in the critical layer of the DVRW. Moreover, there is no sign of nonlinear SI.

To conclude this section, let us briefly address an important technicality. The preceding discussion asserted without proof that the inner part of the excited mode was dominated by a vortex Rossby wave. A vortex Rossby wave should possess the basic characteris-

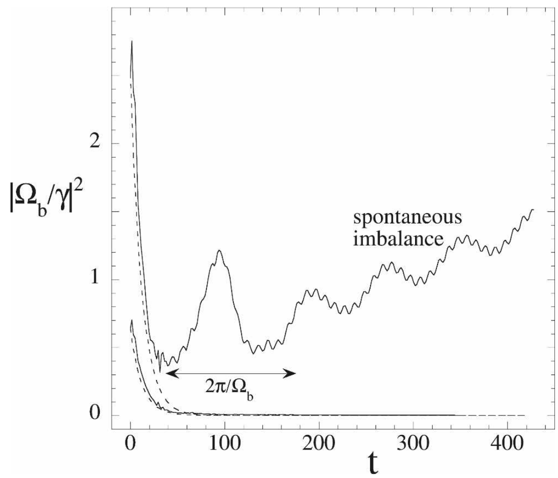

FIG. 7. Conditional SI. The top curve (solid) shows the amplitude of the DVRW in Fig. 6. The horizontal bar (with double arrows) indicates the maximum bounce period of the wave. Since $\Omega_b/|\gamma|$ initially exceeds unity, nonlinear SI occurs. The bottom curve (solid) is from a similar experiment, in which the initial wave amplitude is reduced by a factor of 0.25. Here, there is no sign of SI. The dashed curves are the exponential-decay predictions of linear theory ($\Omega_b^2 \propto e^{\gamma t}$). Time t is measured in units of $\overline{\Omega}_{\max}^{-1}$. The data shown here correspond to simulations G1 (top curve) and G3 (bottom curve) of SM06. The reader may consult this reference for details on the measurement of Ω_b and the calculation of γ.

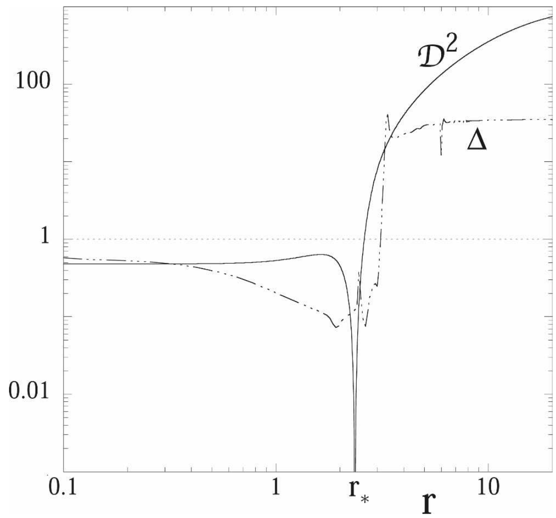

FIG. 8. The radial dependence of balance parameters in the numerical simulation of nonlinear SI (Fig. 6). Both $\mathcal{D}^2$ and Δ (at $t = 429.18$) are less than unity to a radius beyond r_*, suggesting that the DVRW and its critical layer are approximately balanced. In contrast, $\mathcal{D}^2$ and Δ are much greater than unity in the IG wave radiation zone. Radius r is measured in units of the characteristic vortex scale, as were all lengths in Fig. 6.

tics of a balanced perturbation. The formal theory of asymmetric balance requires that

$$\mathcal{D}^2 = \frac{(\omega - n\overline{\Omega})^2}{\overline{\eta}\,\overline{\xi}} \ll 1, \tag{33}$$

in which, as usual, ω is the oscillation frequency of the mode. The weaker condition, $\mathcal{D}^2 < 1$, suffices to ensure that the intrinsic frequency of the mode is less than the local inertial frequency. Figure 8 (solid curve) verifies that the asymmetric balance condition weakly holds in the vortex core and strongly holds in the critical layer. For standard balance (McWilliams 1985; Polvani et al. 1994; Montgomery and Franklin 1998), the central perturbation would normally satisfy

$$\Delta \equiv \frac{\delta_n}{\zeta_n} \ll 1, \tag{34}$$

in which δ_n and ζ_n are the peak values (at a given radius) of the divergence and vorticity components of the mode. Figure 8 (broken curve) indicates that the inner part of the mode satisfies condition (34). On the other hand, neither $\mathcal{D}^2$ nor Δ is less than unity far beyond the critical layer, where the DVRW transitions to an IG wave.

4. The spontaneous imbalance of a dry baroclinic cyclone

The theory of IG wave production by DVRWs, including the influence of critical layers, has been extended to 3D stratified cyclones with barotropic basic states and cloud coverage (SM04; Schecter and Montgomery 2007, hereafter SM07). Plougonven and Zeitlin (2002) had previously developed an analytical theory for IG wave emission by "pancake" vortices, but their analysis did not account for active critical layers. A general theory for baroclinic cyclones, whose tangential winds have vertical shear, was lacking before now. The following extension-by-analogy of shallow-water theory (SM06) to dry baroclinic cyclones has not been tested against numerical experiments, but is presented here for the purpose of motivating a deeper investigation.

As usual, we will assume that θ (the potential temperature) of the atmosphere increases monotonically with altitude and that the axisymmetric PV distribution $\overline{q}(r, \theta)$ of the unperturbed cyclone decreases monotonically with radius on a surface of constant θ. With suitable boundary conditions, such a vortex is stable in the context of balanced dynamics (Montgomery and Shapiro 1995; Ren 1999). On the other hand, stability is not guaranteed when IG waves are allowed to interact with DVRWs—in which case SI can occur.

a. PV and angular pseudomomentum equations

It is most convenient to analyze the dynamics of a baroclinic cyclone using the hydrostatic primitive equations in isentropic coordinates (see Appendix B). The assumption of hydrostatic balance does not permit accurate modeling of high-frequency IG waves. Accordingly, we will confine our attention to IG wave radiation that has a characteristic frequency greater than f but much less than the Brunt–Väisälä frequency N.

There are two prominent equations that we must explicitly consider in order to discuss the SI of a baroclinic MC. The first is the linearized PV equation:

$$\frac{D_V q'}{Dt} = -u'\frac{\partial \overline{q}}{\partial r}. \tag{35}$$

The second is the lowest-order flux conservative equation for the angular pseudomomentum density $\mathcal{J}$. In isentropic coordinates,

$$\mathcal{J} \equiv -\frac{r\overline{\sigma}^2(q')^2}{2(\partial\overline{q}/\partial r)} - r\sigma' \upsilon' \tag{36}$$

and

$$\frac{\partial \mathcal{J}}{\partial t} = \frac{1}{r}\frac{\partial}{\partial r}(r^2\overline{\sigma}u'\upsilon') - \frac{\partial}{\partial\theta}\left(\frac{p'}{g}\frac{\partial\psi'}{\partial\varphi}\right) - \frac{\partial}{\partial\varphi}\left[\frac{\overline{\upsilon}}{r}\mathcal{J} + \frac{\overline{\sigma}}{2}(u'^2 - \upsilon'^2) - \frac{R(p')^2}{2g\overline{p}}\left(\frac{\overline{p}}{p_a}\right)^{R/c_p}\right], \tag{37}$$

in which σ is the isentropic mass density, ψ is the Montgomery streamfunction, g is gravitational acceleration, R is the gas constant of dry air, c_p is the specific heat of dry air at constant pressure p, and p_a is the constant ambient surface pressure (cf. Chen et al. 2003).

The total angular pseudomomentum L in a fixed volume $\mathcal{V}$, containing a compact vortex, is the integral

$$L \equiv \int_{\mathcal{V}} d\varphi\, d\theta\, dr r\mathcal{J}. \tag{38}$$

Let $\mathcal{V}$ be a cylinder of radius R_υ, with top and bottom surfaces at $\theta_{\max}$ and $\theta_{\min}$ (Fig. 9). Integrating Eq. (37) over $\mathcal{V}$, we obtain

$$\frac{dL}{dt} = \int_{-\pi}^{\pi}\int_{\theta_{\min}}^{\theta_{\max}} d\varphi\, d\theta [r^2\overline{\sigma}u'\upsilon']_{r=R_\upsilon} - \int_{-\pi}^{\pi}\int_{0}^{R_\upsilon} d\varphi\, dr r \frac{p'}{g}\frac{\partial\psi'}{\partial\varphi}\Bigg|_{\theta_{\min}}^{\theta_{\max}} \equiv S. \tag{39}$$

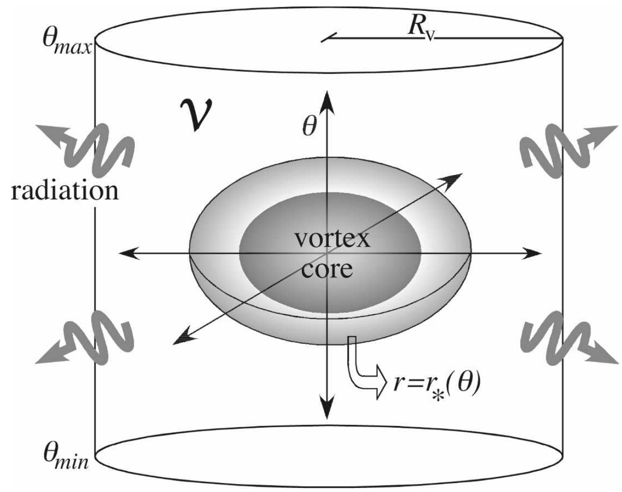

FIG. 9. Illustration of a baroclinic MC and a cylinder that separates the vortex from the environment for analytical purposes. An arbitrary DVRW will emit spiral IG waves into the environment. Isentropic PV stirring in the critical layer, centered on the surface $r = r_*(\theta)$, will potentially damp the DVRW and thereby suppress the IG wave radiation.

The surface integrals that define S are associated with IG wave radiation, and possibly waves that are reflected back into the vortex from distant objects should they exist. Specifically, the top integral is the outward angular momentum flux on the lateral boundary of $\mathcal{V}$ in the absence of ambient rotation [assuming that $\overline{\upsilon} = 0$ at $r = R_\upsilon$; cf. Eq. (B8)]. The bottom integral is the net outward angular momentum flux on the vertical boundaries of $\mathcal{V}$ for any value of f.

Note that we have departed from our previous convention, and have chosen to represent the rate of change of angular pseudomomentum in the environment by S rather than by an indefinite volume integral. This alternative approach will facilitate the derivation of a formula for the growth rate of a radiative DVRW.

b. The growth rate of a DVRW

As in shallow-water theory, a DVRW is here viewed as a nearly balanced vortex mode that matches onto a spiral IG wave in the environment. Presumably, the IG wave emission compels the DVRW to grow. In the outer region of the vortex, there exists a 3D critical layer in which the angular rotation frequency of the cyclone equals the angular phase velocity of the mode (Fig. 9). The PV disturbance in the critical layer is viewed (for the following analysis) as a relatively weak perturbation. Loosely speaking, the isentropic stirring of PV in the critical layer is slaved to the velocity fields of the DVRW and of the mean vortex. At "higher order," the growth of q' in the critical layer compels the

DVRW to decay. The following formally examines the competition between the positive feedback of IG wave radiation and the negative feedback of PV stirring in the critical layer.

In a baroclinic cyclone, the perturbation fields of an ideal DVRW have the form

$$\begin{bmatrix} u'_d \\ v'_d \\ \sigma'_d \\ p'_d \\ \psi'_d \\ q'_d \end{bmatrix} = a(t)e^{i(n\varphi-\omega t)}\begin{bmatrix} U(r,\theta) \\ V(r,\theta) \\ \Sigma(r,\theta) \\ P(r,\theta) \\ \Psi(r,\theta) \\ Q(r,\theta) \end{bmatrix} + \text{c.c.}, \qquad (40)$$

in which the phase of a varies at a much slower rate than ω. Far from the vortex core, the above wavefunctions match onto those of a spiral IG wave.

The critical layer is centered on the surface $r = r_*(\theta)$ in which r_* satisfies the following resonance condition:

$$\overline{\Omega}(r_*, \theta) \equiv \omega/n. \qquad (41)$$

In linear theory, the radial length scale $\delta r_*(\theta)$ of the critical layer is proportional to

$$l_\gamma(\theta) \equiv \left|\frac{\gamma}{n\partial\overline{\Omega}/\partial r}\right|_{r=r_*}, \qquad (42)$$

in which $\gamma \equiv d\ \ln|a|/dt$. In principle, the constant of proportionality is of order unity (cf. Schecter et al. 2000), but a more conservative choice of order 10 is frequently used (SM04; SM06; SM07). If at some vertical level r_* happens to be near the origin, where the radial derivative of $\overline{\Omega}$ vanishes, then a basic extension of the analysis in Schecter et al. (2000) suggests that $\delta r_* \propto \sqrt{|\gamma|}$.

Note that Eq. (40) cannot precisely describe a quasi-mode that is damped by the growth of q' in the region of resonance. In particular, $q' = q'_d$ would be accurate only outside the critical layer. Inside the critical layer, let

$$q' = \tilde{q}_{cl}(r, \theta, t)e^{in\varphi} + \text{c.c.}, \quad |r - r_*(\theta)| < \delta r_*(\theta), \qquad (43)$$

in which $\tilde{q}_{\text{cl}}$ is to be determined.

To find the growth rate of a DVRW, let us first divide the total angular pseudomomentum into DVRW and critical-layer components; that is, let $L = L_d + L_{\text{cl}}$ in which

$$L_d \equiv \int_{-\pi}^{\pi}\int_{\theta_{\min}}^{\theta_{\max}}⨍_0^{R_v} d\varphi\, d\theta\, drr\mathcal{J} \quad \text{and}$$

$$L_{\text{cl}} \equiv \int_{-\pi}^{\pi}\int_{\theta_{\min}}^{\theta_{\max}}\int_{r_*-\delta r_*}^{r_*+\delta r_*} d\varphi\, d\theta\, drr\mathcal{J}. \qquad (44)$$

Here $⨍$ is a radial integral that excludes the critical layer, and the value of R_v corresponds to the inner edge of the radiation zone.[6] With the above decomposition, conservation of total L [Eq. (39)] becomes

$$\frac{dL_d}{dt} = S - \frac{dL_{\text{cl}}}{dt}. \qquad (45)$$

The restructured conservation law [Eq. (45)] is readily transformed into an equation for the amplitude $|a|$ of the DVRW. Inserting Eq. (40) into the integral expression for L_d [Eq. (44)] and taking the time derivative yields

$$\frac{dL_d}{dt} = 2\pi\mathcal{M}\frac{d|a|^2}{dt}, \qquad (46)$$

in which

$$\mathcal{M} \equiv \int_{\theta_{\min}}^{\theta_{\max}}⨍_0^{R_v} d\theta\, dr\left[\frac{r^2\overline{\sigma}^2|Q|^2}{-\partial\overline{q}/\partial r} - r^2(\Sigma V^* + \text{c.c.})\right] \qquad (47)$$

is the angular pseudomomentum of the DVRW divided by $2\pi|a|^2$. Likewise, inserting Eq. (40) into the surface integrals that define S yields

$$S = 4\pi\epsilon_{\text{rad}}|a|^2, \qquad (48)$$

in which

$$\epsilon_{\text{rad}} \equiv \frac{1}{2}\int_{\theta_{\min}}^{\theta_{\max}} d\theta\,(r^2\overline{\sigma}UV^* + \text{c.c.})_{r=R_v} - \frac{1}{2g}\int_0^{R_v} dr(-inrP\Psi^* + \text{c.c})|_{\theta_{\min}}^{\theta_{\max}}. \qquad (49)$$

It is consistent with the barotropic problem (SM04; SM07) to expect positive values for $\mathcal{M}$ and ϵ_{rad}.

A different path is required to evaluate the time derivative of angular pseudomomentum in the critical

[6] Sections 2 and 3 assumed that the angular pseudomomentum of the DVRW was negligible beyond the inner core of the vortex (i.e., for $r > r_* - \delta r_*$). Here, we have taken a more liberal view, and have allowed the angular pseudomomentum density of the DVRW to exist on both sides of the critical layer. In practice, the contribution to L_d from the inner core typically dominates.

layer where q' is potentially deviant. First, we may write

$$\frac{dL_{\mathrm{cl}}}{dt} = 2\pi \int_{\theta_{\min}}^{\theta_{\max}} \int_{r_* - \delta r_*}^{r_* + \delta r_*} d\theta\, dr \times \left[\frac{r^2 \overline{\sigma}^2}{-\partial \overline{q}/\partial r} \frac{\partial}{\partial t} (\tilde{q}_{\mathrm{cl}} \tilde{q}_{\mathrm{cl}}^*) - r^2 \frac{\partial}{\partial t} \overline{\sigma' v'}^{\varphi} \right], \quad (50)$$

in which $\overline{h}^{\varphi}$ is the azimuthal average of h, as in section 3. The integrand contains two terms that we will examine separately.

To begin with, consider the linearized PV equation [Eq. (35)] in the critical layer,

$$\frac{\partial \tilde{q}_{\mathrm{cl}}}{\partial t} + in\overline{\Omega}\tilde{q}_{\mathrm{cl}} = -aUe^{-i\omega t} \frac{\partial \overline{q}}{\partial r}. \quad (51)$$

Here we have used the modal approximation $u' = u'_d$ on the right-hand side. Presumably, nonmodal contributions to u' are negligible if $\partial \overline{q}/\partial r$ is sufficiently weak in the critical layer.[7] For simplicity, suppose that the initial value of $\tilde{q}_{\mathrm{cl}}$ equals zero. Furthermore, suppose that the DVRW is near marginal stability so that a remains approximately constant over many oscillation periods. Then, integration of Eq. (51) yields

$$\frac{\partial}{\partial t} (\tilde{q}_{\mathrm{cl}} \tilde{q}_{\mathrm{cl}}^*) \rightarrow \frac{2\pi |U|^2 (\partial \overline{q}/\partial r)^2}{|n \partial \overline{\Omega}/\partial r|} \delta(r - r_*) |a|^2 \quad (52)$$

for $t \gg \omega^{-1}$ (cf. SM04). The delta-function response is a signature of resonance.

The second term of the integrand of dL_{cl}/dt [Eq. (50)] is proportional to the time derivative of $\overline{\sigma' v'}^{\varphi}$. For the special case of a barotropic cyclone, it has been argued that the integral of this term is negligible (SM04). The argument was built upon a Frobenius analysis of the critical layer disturbance and on numerical evidence. Let us suppose that the second term of dL_{cl}/dt is also negligible in the more general baroclinic problem, and leave rigorous proof for future research.

Inserting Eq. (52) into the right-hand side of Eq. (50) and neglecting the second term yields

$$\frac{dL_{\mathrm{cl}}}{dt} = 4\pi \epsilon_{\mathrm{cl}} |a|^2, \quad (53)$$

in which

$$\epsilon_{\mathrm{cl}} \equiv -\pi \int_{\theta_{\min}}^{\theta_{\max}} d\theta \left(\frac{r^2 |U|^2 \overline{\sigma}^2 \partial \overline{q}/\partial r}{|n \partial \overline{\Omega}/\partial r|} \right)_{r=r_*}. \quad (54)$$

Note that the positive value of ϵ_{cl} increases from zero with the "average" negative value of $\partial \overline{q}/\partial r$ in the critical layer.

Upon substituting Eqs. (46), (48), and (53) into Eq. (45) we obtain

$$\frac{d|a|}{dt} = \gamma |a|, \quad (55)$$

in which[8]

$$\gamma \equiv \frac{\epsilon_{\mathrm{rad}} - \epsilon_{\mathrm{cl}}}{\mathcal{M}}. \quad (56)$$

The first term of the growth rate ($\epsilon_{\mathrm{rad}}/\mathcal{M}$) accounts for the positive feedback of IG wave radiation. The second term ($-\epsilon_{\mathrm{cl}}/\mathcal{M}$) accounts for the negative feedback of PV stirring in the critical layer.

The preceding theory for γ relied on multiple assumptions that may have limited applicability. The least subtle is that the DVRW (should one even exist) is near marginal stability. A small value of γ is required for the presumed length scale separation between the thin critical layer and the bulk of the vortex. It is also required for the time scale separation between the e-folding and oscillation periods of the wave. Despite the imprecision of Eq. (56) in more general circumstances, it still demonstrates that wave–flow resonances can greatly hinder SI in MCs.

5. The potential impact of SI on tropical cyclones

The introduction referred to a theoretical study by Chow and Chan (2003) that estimated an appreciable rate of angular momentum loss by hurricanes due to IG wave radiation. Specifically, they proposed that a spiral IG wave can remove up to 10% of the core angular momentum in one rotation period. To the author's knowledge, there are no numerical studies at this time that irrefutably support the 10% loss estimate.

On the other hand, there is numerical evidence that radiation-driven instabilities of hurricane-like vortices can occur relatively fast (Schecter and Montgomery 2003; SM04; D. Hodyss and D. Nolan 2005, personal

[7] Note that nonmodal (continuum) contributions to u' are expected to dominate at very late times if the DVRW is damped. Nevertheless, we will assume that Eq. (51) stays valid over the time scale of interest.

[8] Growth rate formulas that are similar to Eq. (56) have been numerically verified for DVRWs near marginal stability in moist barotropic MCs (SM07), dry barotropic MCs (SM04), and shallow-water MCs (SM06).

communication). In the following, we will reexamine these instabilities with the goal of calculating the rate at which they remove angular momentum from a vortex. In addition, we will reexamine the magnitude of the spiral bands of vertical velocity that they create in the radiation zone. It has been speculated that such bands might encourage moist convection.

a. *Radiation torque on a Rankine cyclone*

The study that we shall revisit is SM04, which is based on the hydrostatic Boussinesq primitive equations (see appendix C). In the Boussinesq model, the relative angular momentum of a cyclone (per unit mass) is defined by

$$\mathcal{L} \equiv \frac{1}{\pi R_v^2 H} \int_{\mathcal{V}} d\mathbf{x}^3 r v, \tag{57}$$

in which the volume integral is over a cylinder $\mathcal{V}$ of height H and radius R_v. For simplicity, we assume rigid vertical boundaries at $z = 0$ and at $z = H$. Then, the rate of change of angular momentum due to spiral IG wave radiation is given by

$$\frac{d\mathcal{L}}{dt} = -2\overline{u'v'}^{\varphi,z} \tag{58}$$

in which $\overline{h}^{\varphi,z}$ is the average of h over the lateral boundary of the cylinder $\mathcal{V}$ [cf. Eq. (C10) with condition (C7)].

Consider a barotropic Rankine cyclone in which $\overline{v}_m$ is the maximum tangential velocity and R_m is the radius of maximum wind. The unperturbed angular momentum (per unit mass) of this cyclone is

$$\mathcal{L} = \overline{v}_m R_m \left[1 - \frac{1}{2}\left(\frac{R_m}{R_v}\right)^2\right], \tag{59}$$

assuming that $R_v > R_m$. If the Brunt–Väisälä frequency N is constant, the linear modes of any barotropic cyclone have the form

$$\begin{bmatrix} u' \\ v' \\ w' \\ \phi' \end{bmatrix} = a_o e^{\gamma t} e^{i(n\varphi - \omega t)} \begin{bmatrix} U(r)\cos(m\pi z/H) \\ V(r)\cos(m\pi z/H) \\ W(r)\sin(m\pi z/H) \\ \Phi(r)\cos(m\pi z/H) \end{bmatrix} + \text{c.c.}, \tag{60}$$

in which u', v', w', and ϕ' are the radial velocity, azimuthal velocity, vertical velocity, and geopotential perturbations, respectively. The reader may consult appendix C for formulas that relate the velocity wavefunctions to Φ.

Suppose that the perturbation is dominated by a single mode. Furthermore, suppose that

$$a_o = \frac{\varepsilon}{2} \frac{\overline{v}_m}{|U|_{r=R_m}}, \tag{61}$$

such that the initial amplitude of the radial velocity perturbation at $r = R_m$ and $z = 0$ is ε times the maximum tangential wind speed. Then it is readily shown that the initial rate of change of $\mathcal{L}$ satisfies the following equation:

$$\frac{1}{\mathcal{L}} \frac{d\mathcal{L}}{d\tau} = -\frac{\pi\varepsilon^2 \Re[UV^*]_{r=R_v}}{\left[1 - \frac{1}{2}\left(\frac{R_m}{R_v}\right)^2\right] |U|^2_{r=R_m}}, \tag{62}$$

in which $\Re[\ldots]$ is the real part of the quantity in square brackets and τ is time normalized to the vortex rotation period, $2\pi R_m/\overline{v}_m$. The rhs of Eq. (62) is expected to increase monotonically from zero as the rotational Froude number of the cyclone increases from zero to order one (cf. section 3b; Ford 1994a,b; Plougonven and Zeitlin 2002). In other words, at fixed N, the dimensionless radiation torque is expected to increase monotonically with $\overline{v}_m$ into the superspin parameter regime.

For comparison, surface drag would remove angular momentum (per unit mass) from the unperturbed cyclone at the following rate:

$$\left(\frac{d\mathcal{L}}{dt}\right)_s = -\frac{2C_D}{R_v^2 H} \int_0^{R_v} dr r^2 \overline{v}^2, \tag{63}$$

in which C_D is the average dimensionless drag coefficient. For Rankine cyclones, Eq. (63) implies that

$$\frac{1}{\mathcal{L}} \left(\frac{d\mathcal{L}}{d\tau}\right)_s = -\frac{4\pi C_D R_m^3 \left(\frac{R_v}{R_m} - \frac{4}{5}\right)}{R_v^2 H \left[1 - \frac{1}{2}\left(\frac{R_m}{R_v}\right)^2\right]}, \tag{64}$$

again assuming that $R_v > R_m$. The absolute value of the rhs of Eq. (64) provides a threshold on the dimensionless radiation torque, above which IG wave emission supersedes surface drag as an angular momentum sink. Notably, this threshold does not vary with $\overline{v}_m$. If an intense cyclone cannot generate radiation torque above this threshold, neither can a weak cyclone.

b. *Some computational results in the category 5 hurricane parameter regime*

Figure 10 presents key features of the first baroclinic ($m = 1$) SI modes of a barotropic Rankine cyclone. The parameters of the cyclone resemble those of a category 5 hurricane: $\overline{v}_m = 75$ m s^{-1}; $R_m = 50$ km; $H = 10$ km;

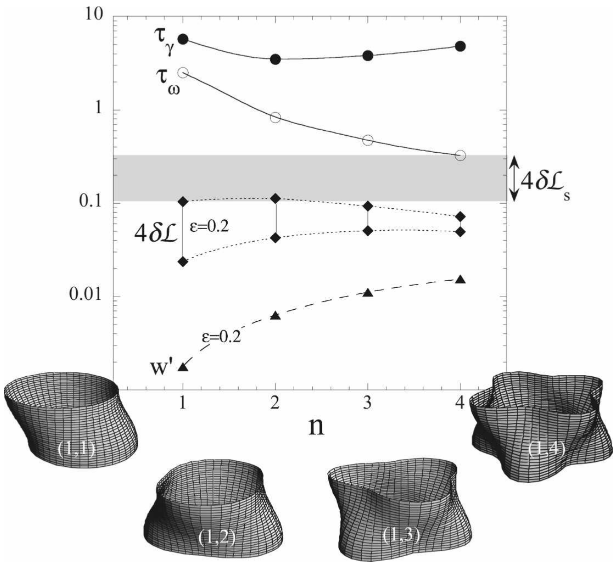

FIG. 10. The SI modes ($m = 1$, $1 \le n \le 4$) of a barotropic Rankine cyclone in the parameter regime of a category 5 hurricane. Each mode consists of an inner DVRW and an outer spiral IG wave. They are initially excited by deforming the isosurfaces of core potential vorticity, as sketched below the graph. The variables τ_γ and τ_ω are, respectively, the *e*-folding time ($1/\gamma$) and oscillation period ($2\pi/\omega$) of the mode, measured in vortex rotation periods ($2\pi R_m/\bar{\upsilon}_m$). The variable $\delta\mathcal{L}$ is the fraction of core relative angular momentum that is lost by radiation in one vortex rotation period. The variable w' is the maximum vertical velocity of the IG wave radiation, normalized to $\bar{\upsilon}_m$. Both $\delta\mathcal{L}$ and w' depend on the instantaneous mode amplitude ε, which is the peak value of u' at the radius of maximum wind, normalized to $\bar{\upsilon}_m$. Here, $\varepsilon = 0.2$. The two curves for $4\delta\mathcal{L}$ correspond to two reasonable definitions of the core radius R_υ (see section 5b). The shaded region covers the estimated range of $4\delta\mathcal{L}_s$, which is (four times) the fraction of core relative angular momentum that would be lost by surface drag over the ocean in one vortex rotation period.

$f = 10^{-4}$ s^{-1}; and $N = 10^{-2}$ s^{-1}.[9] The Rossby and Froude numbers are thus

$$\mathrm{Ro} \equiv \frac{\bar{\upsilon}_m}{fR_m} = 15 \quad \text{and} \quad \mathrm{Fr} \equiv \frac{\pi\bar{\upsilon}_m}{NH} = 2.36, \tag{65}$$

in which NH/π is the characteristic horizontal phase speed of an ambient gravity wave with vertical wavenumber $m = 1$. Each SI mode under consideration, which consists of an inner DVRW and an outer spiral IG wave, corresponds to a numerical solution of the linear eigenmode problem (cf. SM04; appendix C). The eigenmode solver approximated the Rankine cyclone with the following vorticity distribution:

$$\bar{\zeta}(r) = \frac{\bar{\upsilon}_m}{R_m}\left\{1 - \tanh\left[\frac{(r - R_m)}{bR_m}\right]\right\}, \tag{66}$$

in which $b = 0.025$. Two of the four solutions ($n = 2, 4$) were independently verified with numerical integrations of the initial value problem.

The top curves of Fig. 10 show the *e*-folding times and wave periods of the DVRWs and their connected radiation fields. Notably, the *minimum e-folding time is 3.5 rotation periods,* which is just over 4 h. It is important to emphasize that this instability is driven entirely by IG wave radiation. It does not require millions, thousands, hundreds, or even tens of rotation periods to be seen, as would be the case at small Froude number.

The middle curves of Fig. 10 show the fractional loss of core angular momentum ($\delta\mathcal{L}$) in one vortex rotation period [minus the rhs of Eq. (62)]. This quantity increases quadratically with the perturbation strength ε, and is shown for $\varepsilon = 0.2$. The two curves for $\delta\mathcal{L}$ use different values of R_υ. For the top curve, R_υ is chosen to maximize $\delta\mathcal{L}$. All maxima occur in the domain $1.05 < R_\upsilon/R_m < 1.07$. For the bottom curve, $R_\upsilon = r_* + 10l_\gamma$. With this formula, R_υ/R_m decreases from 2.1 to 1.2 as n increases from 1 to 4. For all cases considered,

$$R_\upsilon \ll \frac{NH}{\pi m\gamma}, \tag{67}$$

in which the rhs is an estimate (valid for $\omega \gg f$) of the radial distance that the spiral IG wave travels in one *e*-folding time ($\tau_\gamma = \gamma^{-1}$) of the perturbation. Condition (67) guarantees that $\Re[UV^*]_{r=R\upsilon}$ in Eq. (62) approximately corresponds to the radiation flux created by the core DVRW at the instant under consideration.

Figure 11 (bottom) illustrates the variation of $\delta\mathcal{L}$ with R_υ. The limit as $r \to \infty$ is irrelevant since it is zero. In part, $\delta\mathcal{L}$ vanishes at infinity because the relative angular momentum of a Rankine cyclone diverges with increasing radius. To avoid this problem, we could regularize the vortex. However, the instantaneous radiation field would still decay exponentially with increasing r. Such decay follows from causality; the outer waves were created when the amplitude of the source (the DVRW) was exponentially smaller.

According to Fig. 10, the first baroclinic SI modes of a category 5 "hurricane" do not remove angular momentum at an appreciable rate. For $\varepsilon = 0.2$, the rate is 0.006–0.028 core units per vortex rotation period. As such, it would take between a few days and one week

[9] Using an extratropical value for the Coriolis parameter ($f = 10^{-4}$) instead of a tropical value does not matter, since $\mathrm{Ro} \gg 1$ in either case. Results for $f = 5 \times 10^{-5}$ are nearly indistinguishable from the results presented here.

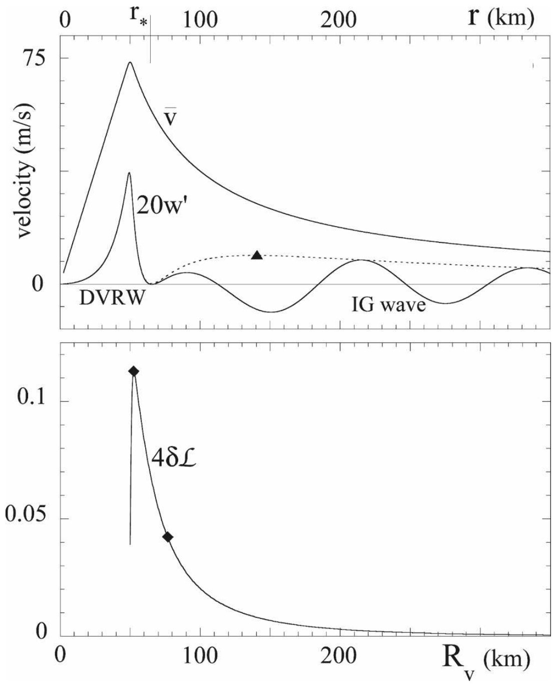

FIG. 11. Snapshot of a radiating "hurricane." The vertical wind (w') and radiation torque ($-\delta\mathcal{L}$) are generated by an SI mode with $(m, n) = (1, 2)$ and $\varepsilon = 0.2$. The solid w' curve is along a fixed azimuth at $z = H/2$. The dashed curve shows the maximum of w' at the same vertical level. Note that w' is negligible in the critical layer [cf. Eq. (C13)]. The dark triangle and diamonds indicate the measurements that were used in Fig. 10.

for spiral radiation to deplete the core circulation ($r \leq R_v$) of the bulk of its original angular momentum, neglecting potential decay of the radiation torque and replenishment by radial inflow. In contrast, Chow and Chan (2003) estimated that $\delta\mathcal{L}$ is of order 0.1. Their large estimate may have resulted from using a small Froude-number formula to approximate the radiation flux at Fr > 1.

For comparison, the shaded region of Fig. 10 shows the estimated fractional loss of core angular momentum due to surface drag ($\delta\mathcal{L}_s$) in one vortex rotation period [minus the rhs of Eq. (64)]. The upper and lower bounds correspond to $C_D = 0.001$ and $C_D = 0.003$, as might be expected for a hurricane over the ocean (cf. Black et al. 2007). The value of R_v was set equal to $1.17R_m$ where $\delta\mathcal{L}_s$ is maximized. The upper bound of the radiation torque barely matches the lower bound of the surface torque. So, it is sensible to assume that radiation torque is typically subdominant. This assumption is a tacit component of current theories for the maximum potential intensity of a hurricane (e.g., Emanuel 1986, 1995).

On another topic, the bottom curves of Fig. 10 show the maximum vertical velocities (w') of the SI modes in the midtropospheric region ($z = H/2$) of the radiation zone ($r > R_v$). For $\varepsilon = 0.2$, these velocities range from 0.002 to 0.015 times $\bar{v}_m$, or from 0.1 to 1.1 m s^{-1}. For perspective, Fig. 11 (top) shows the w' field of the $n = 2$ mode. To the author's knowledge, there is no indisputable evidence from realistic hurricane simulations that the spiral w' bands of SI modes engender deep convection. The case study by Chow et al. (2002) suggests that cloud bands producing little rainwater are more likely. Perhaps future investigations will reveal circumstances in which the IG wave component of an SI mode produces heavy rainbands.

c. Suppression of SI by skirts

Sections 5a and 5b focused on the radiation-driven instability of a Rankine cyclone, which might be exceptional in its propensity for SI. Comprehensive observations (e.g., Mallen et al. 2005) and basic theory (e.g., Emanuel 1986) suggest that, in contrast to the Rankine model, a typical hurricane will have a significant skirt of cyclonic vorticity $\bar{\zeta}$ that extends far beyond R_m and decays with increasing r. The linear theories of sections 3 and 4 suggest that such skirts enhance the damping of DVRWs owing to wave–flow resonances, and thereby hinder SI.

Studies of barotropic MCs in a continuously stratified fluid indicate that the damping power of a skirt is largely controlled by the deformation radius [cf. Eq. (11)]:

$$l_D \equiv \frac{N_m l_z}{\sqrt{\overline{\eta}\,\overline{\xi}}}. \tag{68}$$

Here N_m is the characteristic Brunt–Väisälä frequency of moist air within the cyclone, $\overline{\eta}\overline{\xi}$ is the characteristic inertial stability of the cyclone, and l_z is the vertical length scale of the DVRW. The literature generally indicates that the critical layers of the DVRWs of MCs move radially inward with decreasing l_D (Jones 1995; Reasor and Montgomery 2001; Schecter et al. 2002; Schecter and Montgomery 2003; SM04; SM07; Reasor et al. 2004). Equation (68) indicates that decreasing l_D occurs by

(i) increasing the density of cloud coverage,
(ii) decreasing the positive vertical potential temperature gradient,
(iii) increasing the intensity (inertial stability) of the vortex, or
(iv) decreasing the vertical length scale of the perturbation.

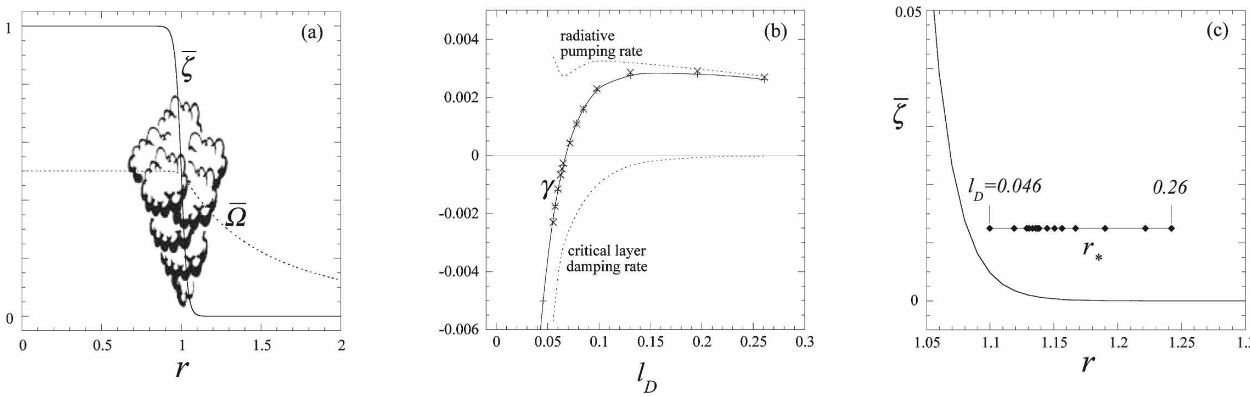

FIG. 12. The suppression of a linear SI mode by increasing cloudiness in a barotropic cyclone at Ro $\equiv \bar{\Omega}_{max}/f = 2$. All lengths are normalized to the radius of maximum wind R_m, and all frequencies are normalized to the peak relative vorticity. (a) Relative vorticity ($\bar{\zeta}$) and angular velocity ($\bar{\Omega}$) of the basic state. The basic state is cloudy in the vicinity of R_m, but the environmental air is dry. (b) The growth rate γ of an $n = 2$ DVRW whose vertical length scale yields $l_D = 0.26R_m$ under dry conditions. As cloudiness increases, l_D decreases and γ ultimately becomes negative. The + symbols correspond to numerical solutions of the eigenmode/quasi-mode problem, and are connected by the solid curve. The dotted curves are theoretical values of the (top) radiative pumping rate and (bottom) critical layer damping rate. Each × corresponds to the sum of the dotted curves at a specific value of l_D. (c) As l_D decreases, the critical radius r_* of the DVRW moves inward, where the vorticity (PV) gradient is relatively steep. Each diamond marks the location of r_* for a data point in (b), with progressively smaller l_D from right to left. Note: the data in (b) and (c) are from Figs. 12 and 10 of SM07.

Typically, the radial PV gradient of a skirt sharply increases with decreasing r. Consequently, decreasing l_D (to values below R_m) greatly increases the negative radial PV gradient in the critical layer of a DVRW and greatly accelerates resonant damping.[10]

Hurricane-like vortices have relatively small values of l_D. For example, evaluating the inertial stability $\overline{\eta\xi}$ at R_m and letting $l_z = H/\pi$, we obtain $l_D = 0.3\ R_m$ for the model hurricane of section 5b. This small value of l_D ensured that the critical layers of all baroclinic DVRWs were centered close to the core; in particular, $r_* \leq 1.6\ R_m$ for each mode. Consequently, in linear theory, a skirt of very modest extension would have sufficed to quench all DVRWs and thereby suppress radiation (cf. SM04).

The above conclusion seems more robust upon considering the effect of moisture. Figure 12, adapted from SM07, illustrates the suppression of a linear SI mode by cloud coverage in a barotropic cyclone. As usual, the SI mode consists of an inner DVRW and an outer spiral IG wave (not shown). The azimuthal wavenumber is $n = 2$, and the vertical wavelength is such that under dry conditions $l_D = 0.26\ R_m$ in which l_D is evaluated at $r = R_m$. Because the cyclone is nearly Rankine, the dry value of l_D is not sufficiently small to quench SI. Nevertheless, l_D is reducible by increasing cloudiness (decreasing N_m) in the vicinity of R_m. As shown here, reduction of l_D by cloud coverage ultimately moves r_* to a location where, in linear theory, critical layer damping prevails over radiative pumping. Interested readers may consult SM07 for further details.[11]

Of course, a steep skirt (or $l_D \ll R_m$) does not guarantee the suppression of SI in a real tropical cyclone; rather, it represents one inhibiting factor. As mentioned earlier, the angular pseudomomentum of a DVRW at sufficiently large amplitude can exceed the finite absorption capacity of its critical layer. In this case, nonlinear SI would occur. Furthermore, hurricanes typically have nonmonotonic cores that suffer shear-flow instabilities. Such instabilities can act as additional sources of spiral IG waves and are not sensitive to the gradient of the skirt. Finally, even if the cyclone has a monotonic potential vorticity distribution, it can exhibit a "nonmodal" shear-flow instability (cf. Nolan and Farrell 1999; Antkowiak and Brancher 2004) that temporarily amplifies the IG wave radiation field. Convective processes within the vortex might initiate such an event.

d. IG wave emission by sheared vortex Rossby waves

If a steep skirt is able to severely damp all DVRWs, then arbitrary forcing might prefer to excite sheared vortex Rossby waves (SVRWs). There is evidence that

[10] Schecter et al. 2002 provides a rare counterexample.

[11] The results in SM07 (section 8) are expressed in terms of a cloudiness parameter ϵ and the dry Rossby deformation radius l_R^{dry}. Here we have used the relation $l_D = (1 - \epsilon)l_D^{dry}$ in which $l_D^{dry} = fl_R^{dry}/\sqrt{\overline{\eta\xi}}$.

such waves exist in tropical cyclones and are capable of generating spiral cloud bands (McDonald 1968; Chen and Yau 2001; Wang 2002a,b; Chen et al. 2003). Balance theories suggest that SVRWs can intensify the storm by fluxing angular momentum to the radius of maximum wind (Montgomery and Kallenbach 1997; Möller and Montgomery 1999, 2000; Enagonio and Montgomery 2001). However, an SVRW may also create IG wave radiation that fluxes angular momentum away from the vortex. Because an SVRW loses coherence and attenuates, it is not likely to sustain radiation by itself. Nevertheless, persistent cycles of SVRW creation and dissipation may engender a notable time-averaged radiation torque.

6. Concluding remarks

This paper reviewed an important paradigm of spontaneous imbalance (SI) that operates at Rossby numbers greater than unity. The main text began by discussing the balanced dynamics of a discrete vortex Rossby wave (DVRW) in a monotonic cyclone (MC). In the context of balanced dynamics, the DVRW is a potential vorticity wave that acts at a distance on fluid beyond the core region of the MC. Section 2 explained that the external flow field of a DVRW most efficiently stirs PV in a critical layer where the angular phase velocity of the wave matches the angular velocity of the mean flow. Since total angular pseudomomentum is conserved, its production in the critical layer damps the DVRW. The damping rate is proportional to the mean radial gradient of critical layer PV.

Beyond the critical layer, balance conditions break down, and the external flow field of the DVRW excites an outward propagating spiral IG wave. Section 3 explained that the DVRW and IG wave have angular pseudomomenta of opposite sign, positive and negative, respectively. Therefore, producing IG wave radiation compels the DVRW to grow. The growth rate due to radiation alone increases algebraically from zero with the rotational Froude number of the vortex.

Nevertheless, SI will occur only if radiative pumping supersedes critical layer damping. The competition between these two processes has been quantified in linear theory, for both shallow-water cyclones [section 3; Eq. (24)] and continuously stratified cyclones [section 4; Eq. (56)]. It is sensible to suppose that increasing Fr would enable or intensify SI because it enhances the radiative pumping of a DVRW. However, increasing Fr at high Rossby number coincides with decreasing the vortex deformation radius l_D. The reduction of l_D moves the critical radius inward where the PV gradient can steepen by orders of magnitude (Fig. 12c). Hence, raising Fr can bolster critical layer damping and suppress SI.

Of course, linear damping does not guarantee suppression. Section 3d showed that nonlinear SI will occur if the angular pseudomomentum of the DVRW exceeds the finite absorption capacity of the critical layer. Such is the case when the bounce frequency Ω_b of the DVRW is greater than the linear decay rate $|\gamma|$. When the wave amplitude is sufficiently large to satisfy this condition, the DVRW mixes the PV distribution in the critical layer and effectively levels the once stabilizing gradient.

Section 5 reexamined SI in the superspin parameter regime where both Ro and Fr are above unity. In particular, it considered the first baroclinic SI modes of a barotropic cyclone at Rossby and Froude numbers characteristic of a category 5 hurricane. It was verified that IG wave radiation can triple the amplitude of a DVRW in just a few vortex rotation periods. However, the negative radiation torque appeared to be less significant than the expected influence of oceanic surface drag.

Despite recent progress, much remains to learn about the SI of intense mesoscale vortices. The extent to which DVRWs (as opposed to continuum perturbations) control IG wave emissions from baroclinic cyclones is unknown. Moreover, the effect of secondary circulation in the basic state is uncertain. The role of moisture is also relatively unexplored. Clearly, moisture cannot be ignored in the troposphere. At the most basic level of approximation, cloud coverage simply reduces the Brunt–Väisälä frequency of the system. As explained in section 5c, this can indirectly enhance the ability of critical layers to inhibit the SI of an MC (cf. SM07). Future research may better explain how a more realistic nonlinear coupling of vortex modes to cloud processes affects their ability to excite IG waves in the far field.

Acknowledgments. This paper was solicited for a special issue on the topics addressed at the SI workshop held in Seattle, Washington, 7–10 August 2006. The SI workshop was sponsored by the National Science Foundation and NorthWest Research Associates. The author thanks Dr. Paul D. Reasor for a helpful discussion regarding section 5. The author also thanks an anonymous referee for helpful suggestions on improving the style of this manuscript. Funding for this research was provided by NSF Grant ATM-0649944, channelled through the Department of Defense, Naval Postgraduate School Grant N00244-07-1-0002.

APPENDIX A

The Shallow-Water Model

The shallow-water equations constitute the simplest model of geophysical flow that accounts for the interaction of vortical motion with IG waves. They form the basis of the theoretical and numerical results of section 3. We may write the shallow-water equations in the following compact form:

$$\frac{\partial \mathbf{u}}{\partial t} + \boldsymbol{\eta} \times \mathbf{u} + \boldsymbol{\nabla}\left(\phi + \frac{\mathbf{u}^2}{2}\right) = 0, \tag{A1}$$

$$\frac{\partial \phi}{\partial t} + \boldsymbol{\nabla} \cdot \phi \mathbf{u} = 0. \tag{A2}$$

Above, $\mathbf{u}$ is the horizontal velocity field, ϕ is the geopotential (gravitational acceleration g times the free surface height), t is time, and $\boldsymbol{\nabla}$ is the horizontal gradient operator. The absolute vorticity vector is defined by

$$\boldsymbol{\eta} \equiv \boldsymbol{\nabla} \times \mathbf{u} + f\hat{\mathbf{z}}, \tag{A3}$$

in which $\hat{\mathbf{z}}$ is the vertical unit vector.

It is well known that Eqs. (A1) and (A2) conserve PV (q) along material trajectories. That is,

$$\frac{\partial q}{\partial t} + \mathbf{u} \cdot \boldsymbol{\nabla} q = 0, \tag{A4}$$

in which

$$q \equiv \frac{\hat{\mathbf{z}} \cdot \boldsymbol{\eta}}{\phi}. \tag{A5}$$

In addition, manipulation of Eqs. (A1) and (A2) yields the following flux-conservation law for absolute angular momentum density:

$$\frac{\partial}{\partial t}\left[\phi\left(rv + \frac{fr^2}{2}\right)\right] = -\boldsymbol{\nabla} \cdot \left[\mathbf{u}\phi\left(rv + \frac{fr^2}{2}\right) + \frac{r\phi^2}{2}\hat{\boldsymbol{\varphi}}\right], \tag{A6}$$

in which r is radius from a central vertical axis, v is the azimuthal velocity field, and $\hat{\boldsymbol{\varphi}}$ is the azimuthal unit vector. Conservation of mass, PV, and absolute angular momentum form the basis of an exact angular pseudomomentum conservation law. The reader may consult Guinn and Schubert (1993) for a detailed derivation.

APPENDIX B

The Hydrostatic Primitive Equations in Isentropic Coordinates

The theoretical results of section 4 are based on the hydrostatic primitive equations in isentropic coordinates. The isentropic coordinate system (e.g., Dutton 1976) replaces the vertical Cartesian coordinate z with the potential temperature

$$\theta \equiv T\left(\frac{p_a}{p}\right)^{R/c_p} \tag{B1}$$

in which T is absolute temperature, R is the gas constant of dry air, c_p is the specific heat of dry air at constant pressure p, and p_a is the ambient surface pressure.

In isentropic coordinates, the momentum equation takes the form

$$\frac{\partial \mathbf{u}}{\partial t} + \eta\hat{\mathbf{z}} \times \mathbf{u} + \boldsymbol{\nabla}_\theta\left(\frac{\mathbf{u}^2}{2} + \psi\right) = 0, \tag{B2}$$

in which $\mathbf{u}$ is the horizontal velocity field, $\boldsymbol{\nabla}_\theta$ is the isentropic horizontal gradient operator, $\eta \equiv \hat{\mathbf{z}} \cdot \boldsymbol{\nabla}_\theta \times \mathbf{u} + f$ is the absolute vertical vorticity, and $\psi \equiv c_pT + gz$ is the Montgomery streamfunction. The hydrostatic relation is given by

$$\frac{\partial \psi}{\partial \theta} = c_p\left(\frac{p}{p_a}\right)^{R/c_p}. \tag{B3}$$

Finally, mass continuity takes the form

$$\frac{\partial \sigma}{\partial t} + \boldsymbol{\nabla}_\theta \cdot \sigma\mathbf{u} = 0, \tag{B4}$$

in which

$$\sigma = -\frac{1}{g}\frac{\partial p}{\partial \theta}. \tag{B5}$$

With appropriate boundary conditions, Eqs. (B2)–(B5) form a closed system.

In the isentropic coordinate system, potential vorticity is given by

$$q \equiv \eta/\sigma \tag{B6}$$

and is conserved along material trajectories; that is,

$$\frac{\partial q}{\partial t} + \mathbf{u} \cdot \boldsymbol{\nabla}_\theta q = 0. \tag{B7}$$

In addition, the absolute angular momentum density is governed by

$$\begin{aligned}\frac{\partial}{\partial t}\left[\sigma\left(rv + \frac{fr^2}{2}\right)\right] = -\boldsymbol{\nabla}_\theta \cdot \Bigg[\mathbf{u}\sigma\left(rv + \frac{fr^2}{2}\right) \\ + \frac{c_prp}{g(1 + c_p/R)}\left(\frac{p}{p_a}\right)^{R/c_p}\hat{\boldsymbol{\varphi}}\Bigg] \\ + \frac{\partial}{\partial \theta}\left(\frac{p}{g}\frac{\partial \psi}{\partial \varphi}\right),\end{aligned} \tag{B8}$$

in which v again represents the azimuthal velocity field. As in shallow-water theory, conservation of mass, PV, and absolute angular momentum form the basis of an exact angular pseudomomentum conservation law.

APPENDIX C

The Hydrostatic Boussinesq Model in Pseudoheight Coordinates

The results of section 5 are based on a hydrostatic Boussinesq model that uses the following pseudoheight as the vertical coordinate:

$$z(p) \equiv \left[1 - \left(\frac{p}{p_a}\right)^{R/c_p}\right]\frac{c_p}{R}\frac{p_a}{\rho_a g}, \tag{C1}$$

in which p_a and ρ_a are ambient surface values of pressure and density (Hoskins and Bretherton 1972). Note that $dz = d\tilde{z}\theta_a/\theta$, in which $\tilde{z}$ is the genuine height coordinate and θ_a is the ambient surface value of potential temperature. The difference between z and $\tilde{z}$ is generally small in the lower 10 km of the atmosphere and vanishes if the stratification is dry adiabatic. Therefore, the pseudo vertical velocity ($w \equiv dz/dt$) of a fluid parcel approximately equals the genuine vertical velocity in the region of interest.

In pseudoheight coordinates, the horizontal momentum equation takes the form

$$\frac{\partial \mathbf{u}}{\partial t} + \mathbf{v}\cdot\nabla\mathbf{u} + f\hat{\mathbf{z}}\times\mathbf{u} + \nabla_z\phi = 0, \tag{C2}$$

in which $\mathbf{u}$ is horizontal velocity, $\mathbf{v} \equiv \mathbf{u} + \hat{\mathbf{z}}w$, $\phi \equiv g\tilde{z}$ is the geopotential, ∇_z is the horizontal gradient operator, and $\nabla \equiv \nabla_z + \hat{\mathbf{z}}\partial/\partial z$. Furthermore, the adiabatic heat equation is given by

$$\frac{\partial\theta}{\partial t} + \mathbf{v}\cdot\nabla\theta = 0. \tag{C3}$$

The hydrostatic relation and mass continuity equations take the forms

$$\theta = \frac{\theta_a}{g}\frac{\partial\phi}{\partial z} \tag{C4}$$

and

$$\nabla\cdot\rho_p\mathbf{v} = 0, \tag{C5}$$

respectively. Above, we have introduced a pseudodensity, defined by

$$\rho_p(z) \equiv \rho_a\left(\frac{p}{p_a}\right)^{c_v/c_p}. \tag{C6}$$

In the Boussinesq approximation, ρ_p is treated as a constant in (C5) and divided through on both sides to obtain

$$\nabla\cdot\mathbf{v} = 0. \tag{C7}$$

With appropriate boundary conditions, Eqs. (C2)–(C4) and (C7) form a closed system.

It can be shown that the Boussinesq equations conserve the following potential vorticity,

$$q(\mathbf{x},t) \equiv (\nabla\times\mathbf{u} + f\hat{\mathbf{z}})\cdot\nabla\theta, \tag{C8}$$

along material trajectories. That is,

$$\frac{\partial q}{\partial t} + \mathbf{v}\cdot\nabla q = 0. \tag{C9}$$

In addition, the relative angular momentum per unit mass is governed by

$$\frac{\partial(rv)}{\partial t} + \nabla\cdot\left[\mathbf{v}\left(rv + \frac{fr^2}{2}\right) + r\phi\hat{\boldsymbol{\varphi}}\right] = 0 \tag{C10}$$

in which v (as usual) is the azimuthal velocity field. SM04 derives an exact angular pseudomomentum conservation law that stems from Eqs. (C9) and (C10). Equation (58) of the main text follows from Eq. (C10), Eq. (C7), and rigid, frictionless vertical boundary conditions.

It is straightforward to derive linearized perturbation equations from the above model. Suppose that the basic state is a barotropic cyclone in gradient balance, and that the vertical boundaries are rigid. Furthermore, suppose that the Brunt–Väisälä frequency $N = \sqrt{\partial^2\overline{\phi}/\partial z^2}$ is constant. Then, the eigenmodes are formally given by Eq. (60) of the main text. Furthermore, it has been shown (SM04) that the geopotential eigenfunction must satisfy the following equation:

$$\frac{1}{r}\frac{d}{dr}\left[\frac{r}{\overline{\eta}\,\overline{\xi} - \hat{\omega}^2}\frac{d}{dr}\Phi\right] - \frac{n}{\hat{\omega}r}\frac{d}{dr}\left[\frac{\overline{\xi}}{\overline{\eta}\,\overline{\xi} - \hat{\omega}^2}\right]\Phi - \left[\frac{n^2}{r^2(\overline{\eta}\,\overline{\xi} - \hat{\omega}^2)} + \left(\frac{m\pi}{NH}\right)^2\right]\Phi = 0, \tag{C11}$$

in which

$$\hat{\omega}(r) \equiv \omega_c - n\overline{\Omega} \tag{C12}$$

and $\omega_c \equiv \omega + i\gamma$ is the complex eigenfrequency. The polarization equations are

$$U(r) = \frac{i}{\overline{\eta}\,\overline{\xi} - \hat{\omega}^2}\left(\hat{\omega}\frac{d\Phi}{dr} - \frac{n\overline{\xi}}{r}\Phi\right),$$

$$V(r) = \frac{1}{\overline{\eta}\,\overline{\xi} - \hat{\omega}^2}\left(\overline{\eta}\frac{d\Phi}{dr} - \frac{n\hat{\omega}}{r}\Phi\right),$$

$$W(r) = \frac{im\pi\hat{\omega}}{HN^2}\Phi \tag{C13}$$

for the radial, azimuthal, and vertical velocities, respectively. The boundary conditions that determine the possible values of ω_c are regularity at the origin and outward IG wave propagation as r tends toward infinity (SM04). The eigenmodes of section 5 were obtained numerically with a radiation condition imposed at $r = 9.5R_m$.

REFERENCES

Antkowiak, A., and P. Brancher, 2004: Transient energy growth for the Lamb-Oseen vortex. *Phys. Fluids,* **16,** L1–L4 doi:10.1063/1.1626123.

Bachman, D. A., 1998: Nonlinear phenomena in a pure electron plasma studied with a 2D fluid code. Ph.D. dissertation, California Institute of Technology, 143 pp.

Balmforth, N. J., S. G. Llewellyn Smith, and W. R. Young, 2001: Disturbing vortices. *J. Fluid Mech.,* **426,** 95–133.

Bassom, A. P., and A. D. Gilbert, 1998: The spiral wind-up of vorticity in an inviscid planar vortex. *J. Fluid Mech.,* **371,** 109–140.

Benilov, E. S., 2005: The effect of ageostrophy on the stability of thin oceanic vortices. *Dyn. Atmos. Oceans,* **39,** 211–226.

Black, P. G., and Coauthors, 2007: Air–sea exchange in hurricanes: Synthesis of observations from the Coupled Boundary Layer Air–Sea Transfer Experiment. *Bull. Amer. Meteor. Soc.,* **88,** 357–374.

Briggs, R. J., J. D. Daugherty, and R. H. Levy, 1970: Role of Landau damping in crossed-field electron beams and inviscid shear flow. *Phys. Fluids,* **13,** 421–432.

Broadbent, E. G., and D. W. Moore, 1979: Acoustic destabilization of vortices. *Philos. Trans. Roy. Soc. London,* **A290,** 353–371.

Brunet, G., and M. T. Montgomery, 2002: Vortex Rossby waves on smooth circular vortices: I. Theory. *Dyn. Atmos. Oceans,* **35,** 153–177.

Cass, A. C., 1998: Experiments on vortex symmetrization in magnetized electron columns. Ph.D. dissertation, University of California, San Diego, 64 pp.

Chan, W. M., K. Shariff, and T. H. Pulliam, 1993: Instabilities of two-dimensional inviscid compressible vortices. *J. Fluid Mech.,* **253,** 173–209.

Charney, J. G., 1948: On the scale of atmospheric motions. *Geophys. Publ.,* **17,** 1–17.

Chen, Y., and M. K. Yau, 2001: Spiral bands in a simulated hurricane. Part I: Vortex Rossby wave verification. *J. Atmos. Sci.,* **58,** 2128–2145.

——, G. Brunet, and M. K. Yau, 2003: Spiral bands in a simulated hurricane. Part II: Wave activity diagnostics. *J. Atmos. Sci.,* **60,** 1239–1256.

Chimonas, G., and H. M. Hauser, 1997: The transfer of angular momentum from vortices to gravity swirl waves. *J. Atmos. Sci.,* **54,** 1701–1711.

Chow, K. C., and K. L. Chan, 2003: Angular momentum transports by moving spiral waves. *J. Atmos. Sci.,* **60,** 2004–2009.

——, ——, and A. K. H. Lau, 2002: Generation of moving spiral bands in tropical cyclones. *J. Atmos. Sci.,* **59,** 2930–2950.

Corngold, N. R., 1995: Linear response of the two-dimensional pure electron plasma: Quasi-modes for some model profiles. *Phys. Plasmas,* **2,** 620–628.

Davidson, R. C., 1990: *Physics of Nonneutral Plasmas.* Addison-Wesley, 733 pp.

Dutton, J. A., 1976: *The Ceaseless Wind: An Introduction to the Theory of Atmospheric Motion.* McGraw-Hill, 579 pp.

Emanuel, K. A., 1986: An air-sea interaction theory for tropical cyclones. Part I: Steady state maintenance. *J. Atmos. Sci.,* **43,** 585–604.

——, 1995: Sensitivity of tropical cyclones to surface exchange coefficients and a revised steady state model incorporating eye dynamics. *J. Atmos. Sci.,* **52,** 3969–3976.

Enagonio, J., and M. T. Montgomery, 2001: Tropical cyclogenesis via convectively forced vortex Rossby waves in a shallow-water primitive equation model. *J. Atmos. Sci.,* **58,** 685–706.

Ford, R., 1994a: The instability of an axisymmetric vortex with monotonic potential vorticity in rotating shallow water. *J. Fluid Mech.,* **280,** 303–334.

——, 1994b: The response of a rotating ellipse of uniform potential vorticity to gravity wave radiation. *Phys. Fluids,* **6,** 3694–3704.

——, M. E. McIntyre, and W. A. Norton, 2000: Balance and the slow quasi-manifold: Some explicit results. *J. Atmos. Sci.,* **57,** 1236–1254.

——, ——, and ——, 2002: Reply. *J. Atmos. Sci.,* **59,** 2878–2882.

Griffiths, M., and M. J. Reeder, 1996: Stratospheric inertia-gravity waves generated in a numerical model of frontogenesis. I: Model solutions. *Quart. J. Roy. Meteor. Soc.,* **122,** 1153–1174.

Guinn, T. A., and W. H. Schubert, 1993: Hurricane spiral bands. *J. Atmos. Sci.,* **50,** 3380–3403.

Haynes, P. H., 1988: Forced, dissipative generalizations of finite amplitude wave-activity conservation relations for zonal and nonzonal basic flows. *J. Atmos. Sci.,* **45,** 2352.

Hoskins, B. J., and F. P. Bretherton, 1972: Atmospheric frontogenesis models: Mathematical formulation and solution. *J. Atmos. Sci.,* **29,** 11–37.

——, 1975: The geostrophic momentum approximation and the semigeostrophic equations. *J. Atmos. Sci.,* **32,** 233–242.

——, M. E. McIntyre, and A. W. Robertson, 1985: On the use and significance of isentropic potential vorticity maps. *Quart. J. Roy. Meteor. Soc.,* **111,** 877–946.

Howe, M. S., 2003: *The Theory of Vortex Sound.* Cambridge University Press, 216 pp.

Jones, S. C., 1995: The evolution of vortices in vertical shear. I: Initially barotropic vortices. *Quart. J. Roy. Meteor. Soc.,* **121,** 821–851.

Kelvin, Lord, 1880: On the vibrations of a columnar vortex. *Philos. Mag.,* **10,** 155–168.

Killworth, P. D., and M. E. McIntyre, 1985: Do Rossby-wave critical layers absorb, reflect, or over-reflect? *J. Fluid Mech.,* **161,** 449–492.

Kop'ev, V. F., and E. A. Leont'ev, 1983: Acoustic instability of an axial vortex. *Sov. Phys. Acoust.,* **29,** 111–115.

——, and ——, 1985: Energy aspect of the acoustic instability of certain steady-state vortices. *Sov. Phys. Acoust.,* **31,** 205–207.

——, and ——, 1988: Acoustic instability of planar vortex flows with circular streamlines. *Sov. Phys. Acoust.,* **34,** 276–278.

Landau, L., 1946: On the vibration of the electronic plasma. *J. Phys. U.S.S.R.,* **10,** 25.

Lansky, I. M., T. M. O'Neil, and D. A. Schecter, 1997: A theory of vortex merger. *Phys. Rev. Lett.,* **79,** 1479–1482.

Le Dizes, S., 2000: Non-axisymmetric vortices in two-dimensional flows. *J. Fluid Mech.,* **406,** 175–198.

Mallen, K. J., M. T. Montgomery, and B. Wang, 2005: Reexamining the near-core radial structure of the tropical cyclone primary circulation: Implications for vortex resiliency. *J. Atmos. Sci.,* **62,** 408–425.

Maslowe, S. A., 1986: Critical layers in shear flow. *Annu. Rev. Fluid. Mech.,* **18,** 405–432.

McDonald, N. J., 1968: The evidence for the existence of Rossby-like waves in the hurricane vortex. *Tellus,* **20,** 138–150.

McIntyre, M. E., 1981: On the 'wave-momentum' myth. *J. Fluid Mech.,* **106,** 331–347.

McWilliams, J. C., 1985: A uniformly valid model spanning the regimes of geostrophic and isotropic, stratified turbulence: Balanced turbulence. *J. Atmos. Sci.,* **42,** 1773–1774.

——, L. P. Graves, and M. T. Montgomery, 2003: A formal theory for vortex Rossby waves and vortex evolution. *Geophys. Astrophys. Fluid Dyn.,* **97,** 275–309.

Möller, J. D., and M. T. Montgomery, 1999: Vortex Rossby waves and hurricane intensification in a barotropic model. *J. Atmos. Sci.,* **56,** 1674–1687.

——, and ——, 2000: Tropical cyclone evolution via potential vorticity anomalies in a three-dimensional balance model. *J. Atmos. Sci.,* **57,** 3366–3387.

——, and L. J. Shapiro, 2002: Balanced contributions to the intensification of Hurricane Opal as diagnosed from a GFDL model forecast. *Mon. Wea. Rev.,* **130,** 1866–1881.

Montgomery, M. T., and R. J. Kallenbach, 1997: A theory of vortex Rossby-waves and its application to spiral bands and intensity changes in hurricanes. *Quart. J. Roy. Meteor. Soc.,* **123,** 435–465.

——, and C. Lu, 1997: Free waves in barotropic vortices. Part I: Eigenmode structure. *J. Atmos. Sci.,* **54,** 1868–1885.

——, and J. L. Franklin, 1998: An assessment of the balance approximation in hurricanes. *J. Atmos. Sci.,* **55,** 2193–2200.

——, and L. J. Shapiro, 1995: Generalized Charney–Stern and Fjortoft theorems for rapidly rotating vortices. *J. Atmos. Sci.,* **52,** 1829–1833.

Muraki, D. J., C. Snyder, and R. Rotunno, 1999: The next-order corrections to quasigeostrophic theory. *J. Atmos. Sci.,* **56,** 1547–1560.

Nolan, D. S., and B. F. Farrell, 1999: Generalized stability analyses of asymmetric disturbances in one- and two-celled vortices maintained by radial inflow. *J. Atmos. Sci.,* **56,** 1282–1307.

O'Neil, T. M., 1965: Collisionless damping of nonlinear plasma oscillations. *Phys. Fluids,* **8,** 2255–2262.

O'Sullivan, D., and T. J. Dunkerton, 1995: Generation of inertia–gravity waves in a simulated life cycle of baroclinic instability. *J. Atmos. Sci.,* **52,** 3695–3705.

Papaloizou, J. C. B., and J. E. Pringle, 1987: The dynamic stability of differentially rotating discs—III. *Mon. Not. Roy. Astron. Soc.,* **225,** 267–283.

Pillai, S., and R. W. Gould, 1994: Damping and trapping in 2D inviscid fluids. *Phys. Rev. Lett.,* **73,** 2849–2852.

Plougonven, R., and V. Zeitlin, 2002: Internal gravity wave emission from a pancake vortex: An example of wave-vortex interaction in strongly stratified flows. *Phys. Fluids,* **14,** 1259–1268.

——, and C. Snyder, 2005: Gravity waves excited by jets: Propagation versus generation. *Geophys. Res. Lett.,* **32,** L18802, doi:10.1029/2005GL023730.

Polvani, L. M., J. C. McWilliams, M. A. Spall, and R. Ford, 1994: The coherent structures of shallow-water turbulence: Deformation-radius effects, cyclone/anticyclone asymmetry and gravity-wave generation. *Chaos,* **4,** 177–186.

Reasor, P. D., and M. T. Montgomery, 2001: Three-dimensional alignment and co-rotation of weak, TC-like vortices via linear vortex-Rossby-waves. *J. Atmos. Sci.,* **58,** 2306–2330.

——, ——, and L. D. Grasso, 2004: A new look at the problem of tropical cyclones in shear flow: Vortex resiliency. *J. Atmos. Sci.,* **61,** 3–22.

Reeder, M. J., and M. Griffiths, 1996: Stratospheric inertia-gravity waves generated in a numerical model of frontogenesis. II: Wave sources, generation mechanisms and momentum fluxes. *Quart. J. Roy. Meteor. Soc.,* **122,** 1175–1195.

Ren, S., 1999: Further results on the stability of rapidly rotating vortices in the asymmetric balance formulation. *J. Atmos. Sci.,* **56,** 475–482.

Rossi, L. F., J. F. Lingevitch, and A. J. Bernoff, 1997: Quasi-steady monopole and tripole attractors for relaxing vortices. *Phys. Fluids,* **9,** 2329–2338.

Saujani, S., and T. G. Shepherd, 2002: Comments on "Balance and the slow quasimanifold: Some explicit results." *J. Atmos. Sci.,* **59,** 2874–2877.

Schecter, D. A., D. H. E. Dubin, A. C. Cass, C. F. Driscoll, I. M. Lansky, and T. M. O'Neil, 2000: Inviscid damping of asymmetries on a two-dimensional vortex. *Phys. Fluids,* **12,** 2397–2412.

——, and M. T. Montgomery, 2003: On the symmetrization rate of an intense geophysical vortex. *Dyn. Atmos. Oceans,* **37,** 55–87.

——, and ——, 2004: Damping and pumping of a vortex Rossby wave in a monotonic cyclone: Critical layer stirring versus inertia-buoyancy wave emission. *Phys. Fluids,* **16,** 1334–1348.

——, and ——, 2006: Conditions that inhibit the spontaneous radiation of spiral inertia–gravity waves from an intense mesoscale cyclone. *J. Atmos. Sci.,* **63,** 435–456.

——, and ——, 2007: Waves in a cloudy vortex. *J. Atmos. Sci.,* **64,** 314–337.

——, ——, and P. D. Reasor, 2002: A theory for the vertical alignment of a quasigeostrophic vortex. *J. Atmos. Sci.,* **59,** 150–168.

——, M. E. Nicholls, J. Persing, A. J. Bedard Jr., and R. A. Pielke Sr., 2008: Infrasound emitted by tornado-like vortices: Basic theory and a numerical comparison to the acoustic radiation of a single-cell thunderstorm. *J. Atmos. Sci.,* **65,** 685–713.

Shapiro, L. J., and M. T. Montgomery, 1993: A three-dimensional balance theory for rapidly rotating vortices. *J. Atmos. Sci.,* **50,** 3322–3335.

Shepherd, T. G., 2003: Hamiltonian dynamics. *Encyclopedia of Atmospheric Sciences,* J. R. Holton, J. A. Curry, and J. A. Pyle, Eds., Academic Press, 929–938.

Shukhman, I. G., 1991: Nonlinear evolution of spiral density waves generated by the instability of the shear layer in a rotating compressible fluid. *J. Fluid Mech.,* **233,** 587–612.

Snyder, C., W. C. Skamarock, and R. Rotunno, 1993: Frontal dynamics near and following frontal collapse. *J. Atmos. Sci.,* **50,** 3149–3212.

Spencer, R. L., and S. N. Rasband, 1997: Damped diocotron quasi-modes of nonneutral plasmas and inviscid fluids. *Phys. Plasmas,* **4,** 53–60.

Vanneste, J., and I. Yavneh, 2004: Exponentially small inertia–gravity waves and the breakdown of quasigeostrophic balance. *J. Atmos. Sci.,* **61,** 211–223.

Wang, Y., 2002a: Vortex Rossby waves in a numerically simulated tropical cyclone. Part I: Overall structure, potential vorticity, and kinetic energy budgets. *J. Atmos. Sci.,* **59,** 1213–1238.

——, 2002b: Vortex Rossby waves in a numerically simulated tropical cyclone. Part II: The role in tropical cyclone structure and intensity changes. *J. Atmos. Sci.,* **59,** 1239–1262.

Zeitlin, V., 1991: On the backreaction of acoustic radiation for distributed two-dimensional vortex structures. *Phys. Fluids A,* **3,** 1677–1680.

Zhang, F., 2004: Generation of mesoscale gravity waves in upper-tropospheric jet-front systems. *J. Atmos. Sci.,* **61,** 440–457.